




Article

# The Hexacoordinate Si Complex $\text{SiCl}_4(4\text{-Azidopyridine})_2$ —Crystallographic Characterization of Two Conformers and Probing the Influence of $\text{SiCl}_4$ -Complexation on a Click Reaction with Phenylacetylene

Sophie Riedel<sup>1</sup>, Maik Gerwig<sup>1</sup>, Daniela Gerlach<sup>1</sup>, Erica Brendler<sup>2</sup> , Robert Gericke<sup>3</sup> , Edwin Kroke<sup>1,4</sup> and Jörg Wagler<sup>1,\*</sup> 

<sup>1</sup> Institut für Anorganische Chemie, TU Bergakademie Freiberg, D-09596 Freiberg, Germany; sophie.riedel@chemie.tu-freiberg.de (S.R.); maikgerwig@gmx.de (M.G.); d\_gerlach@gmx.de (D.G.); edwin.kroke@chemie.tu-freiberg.de (E.K.)

<sup>2</sup> Institut für Analytische Chemie, TU Bergakademie Freiberg, D-09596 Freiberg, Germany; erica.brendler@chemie.tu-freiberg.de

<sup>3</sup> Institute of Resource Ecology, Helmholtz-Zentrum Dresden-Rossendorf eV, D-01328 Dresden, Germany

<sup>4</sup> Zentrum für effiziente Hochtemperaturstoffwandlung (ZeHS), TU Bergakademie Freiberg, D-09596 Freiberg, Germany

\* Correspondence: joerg.wagler@chemie.tu-freiberg.de; Tel.: +49-3731-39-4343



**Citation:** Riedel, S.; Gerwig, M.; Gerlach, D.; Brendler, E.; Gericke, R.; Kroke, E.; Wagler, J. The Hexacoordinate Si Complex  $\text{SiCl}_4(4\text{-Azidopyridine})_2$ —Crystallographic Characterization of Two Conformers and Probing the Influence of  $\text{SiCl}_4$ -Complexation on a Click Reaction with Phenylacetylene. *Inorganics* **2023**, *11*, 473. <https://doi.org/10.3390/inorganics11120473>

Academic Editors: David Morales-Morales and Debbie C. Crans

Received: 30 October 2023

Revised: 27 November 2023

Accepted: 1 December 2023

Published: 5 December 2023



**Copyright:** © 2023 by the authors. Licensee MDPI, Basel, Switzerland. This article is an open access article distributed under the terms and conditions of the Creative Commons Attribution (CC BY) license (<https://creativecommons.org/licenses/by/4.0/>).

**Abstract:** 4-Azidopyridine (**1**) and  $\text{SiCl}_4$  react with the formation of the hexacoordinate silicon complex  $\text{SiCl}_4(4\text{-azidopyridine})_2$  (**2**). Upon dissolving in warm chloroform, the complex dissociates into the constituents **1** and  $\text{SiCl}_4$  and forms back upon cooling. Depending on the cooling, two different crystalline modifications of **2** were obtained, which feature two different *trans*-conformers. Slow cooling to room temperature afforded conformer **2'**, which features coplanar pyridine rings. Rapid cooling to  $-39^\circ\text{C}$  afforded crystals of conformer **2''**, in which the planes of the pyridine ligands are nearly orthogonal to one another. Whereas **2'** resembles the molecular arrangement of various other known  $\text{SiX}_4(\text{pyridine})_2$  ( $X = \text{halide}$ ) complexes, **2''** represents the first crystallographically confirmed example of a  $\text{SiX}_4(\text{pyridine})_2$  complex in this conformation. Conformers **2'** and **2''** were studied with  $^{13}\text{C}$  and  $^{29}\text{Si}$  solid state NMR spectroscopy. Their differences in  $^{29}\text{Si}$  chemical shift anisotropy, as well as energetic differences, were further investigated with computational analyses. In spite of the similar stabilities of the two conformers as isolated molecules, the crystal packing of **2''** is less stable, and its crystallization is interpreted as a kinetically controlled effect of seed formation. (3+2)-cycloaddition of **1** and phenylacetylene in toluene at  $110^\circ\text{C}$  yields a mixture of 1-(4-pyridyl)-4-phenyl-1,2,3-triazole (1,4-3) and 1-(4-pyridyl)-5-phenyl-1,2,3-triazole (1,5-3) in approximate 1:2 molar ratio. The crystal structures of the two isomers were determined via X-ray diffraction. In chloroform (at  $60^\circ\text{C}$ ), this reaction is slow (less than 2% conversion within 4 h), but the presence of  $\text{SiCl}_4$  enhanced the rate of the reaction slightly, and it shifted the triazole isomer ratio to ca. 1:6 in favor of 1,5-3.

**Keywords:** chemical shift anisotropy; (3+2)-cycloaddition; Hirshfeld surface analysis; hypercoordination; packing efficiency; polymorphism; silicon; triazole

## 1. Introduction

In the exploration of the chemistry of hypercoordinate silicon compounds [1–6], i.e., compounds with penta-, hexa- or even higher coordinated silicon atoms, a Lewis acid-base adduct of a silicon halide and simple *N*-donor ligand played a pioneering role. The complex  $\text{SiF}_4(\text{NH}_3)_2$  has been reported in the literature more than two centuries ago [7]. Its crystallographic analysis confirmed the *trans*-arrangement of the two monodentate *N*-donor ligands

(i.e., ammonia molecules) in the octahedral Si coordination sphere [8]. The binding of chelating bidentate diamines (such as *N,N,N',N'*-tetramethylethylenediamine, TMEDA) to silicon halides may yield hexacoordinate Si complexes with *cis*-arrangement of the *N*-donor ligands (e.g., in  $\text{SiF}_4(\text{TMEDA})$  [9] and  $\text{SiCl}_4(\text{TMEDA})$  [10]). Related silicon coordination chemistry with pyridine derivatives gave rise to a variety of related Lewis acid-base adducts, i.e., for silanes with monodentate Si-bound substituents *X* the coordination of two molecules of monodentate pyridines at various silanes afforded hexacoordinate Si complexes with *trans*-arrangement of the *N*-donors (type **A** in Figure 1, e.g., with  $R, X_4 = \text{H}, \text{F}_4$  [11], 4-Ph,  $\text{F}_4$  [12],  $\text{H}, \text{Cl}_4$  [13], 4-Me,  $\text{Cl}_n\text{Br}_{4-n}$  [14], 3,5-Me<sub>2</sub>,  $\text{Br}_4$  [15],  $\text{H}, \text{Cl}_3(\text{OSiCl}_3)$  [16], 4-Et,  $\text{H}_2\text{Cl}_2$  [17], 3-Me,  $\text{H}_2\text{Cl}_2$  [18], 4-Me,  $\text{HMeCl}_2$  [19]). Chelating bidentate pyridine derivatives, such as 2,2'-bipyridyl (bipy) or phenanthroline (phen), afforded complexes with *cis*-arranged *N*-donors (type **B**, e.g.,  $\text{SiF}_4(\text{bipy})$  [20],  $\text{SiF}_3(\text{CCPh})(\text{bipy})$  [21],  $\text{Si}(\text{C}_2\text{F}_5)_2(\text{OPh})_2(\text{phen})$  [22],  $\text{SiCl}_2\text{H}_2(\text{bipy})$  [23],  $\text{Si}(\text{NCS})_4(\text{bipy})$  [24], and  $\text{Si}(\text{NCO})_4(\text{phen})$  [25]). In some cases, excess *N*-donor ligands may bind to the Si atom with ionic dissociation of two Si-bound substituents and with retention of the Si coordination number 6. For monodentate pyridine ligands, the formation of ionic complexes of the type **C** was observed, in which the remaining monodentate substituents *X* are *trans* (e.g., with  $R, X_2 = 3\text{-Me}, \text{H}_2$  [26], 4-Me,  $\text{Cl}_2$  [27]). For related complexes with chelating bidentate *N*-donor ligands, the formation of complexes of type **D** was observed (e.g.,  $[\text{SiCl}_2(\text{bipy})_2]^{2+}$  [28],  $[\text{Si}(\text{OH})_2(\text{bipy})_2]^{2+}$  [29],  $[\text{Si}(\text{OMe})_2(\text{phen})_2]^{2+}$  [30]).

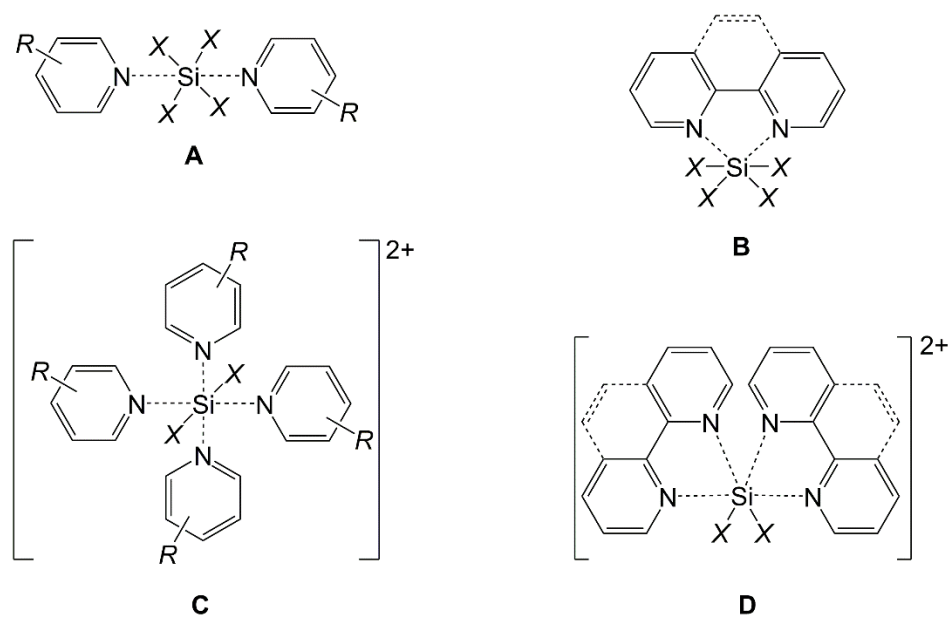


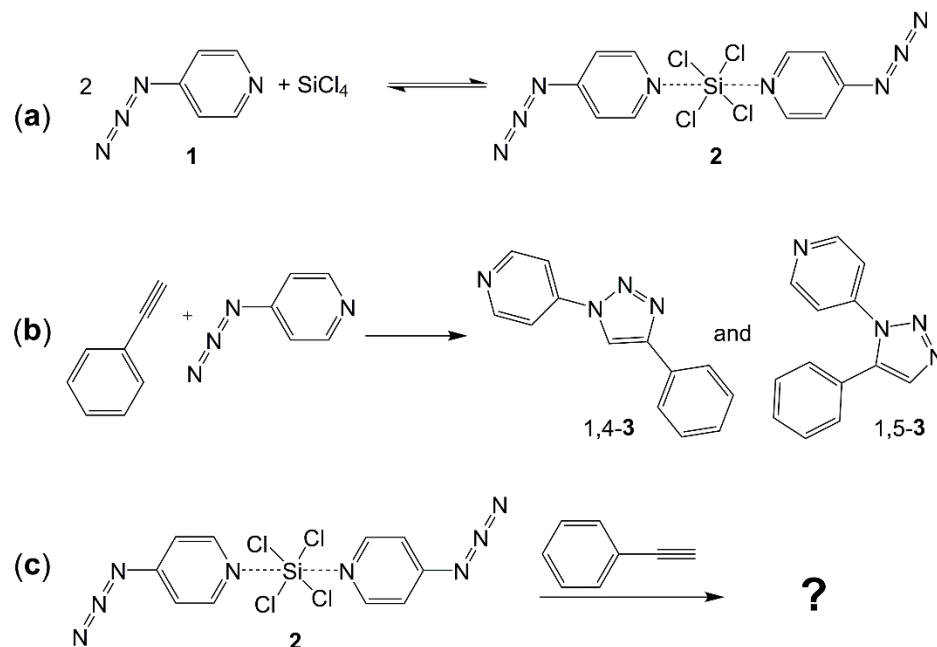
**Figure 1.** Generic representation of some different classes of silicon complexes with pyridine ligands (neutral complexes **A** and cationic complexes **C**) and with bipyridyl or phenanthroline type ligands (neutral complexes **B** and cationic complexes **D**). The Si-bound groups *X* and the ligand-bound substituents *R* are specified in the text for particular examples.

In addition to these classes **A**, **B**, **C**, and **D** of pyridine-Si complexes, other coordination motifs have also been encountered, such as the mono-cationic pentacoordinate Si complex  $[\text{SiHMeBr}(4\text{-methylpyridine})_2]^+$  [31], and other pyridine derivatives have been engaged in silicon coordination chemistry as well, e.g., terpyridines [32].

Furthermore, some Si complexes of type **B** are particularly interesting because of their  $\text{SiN}_6$  coordination sphere and their particularly nitrogen-rich Si environment, which originates from Si-bound azido and tetrazolato groups:  $[\text{Si}(\text{N}_3)_4(\text{phen})]$  [33],  $[\text{Si}(\text{N}_3)_2(\text{tetrazolato})_2(\text{bipy})]$  [34]. The latter were obtained via (3+2)-cycloaddition reactions of nitriles and Si-bound azido groups.

As silicon complexes with azido-functionalized pyridine backbone have not been reported in the literature yet, and related click-chemistry thereof (facile (3+2)-cycloaddition

reactions) [35] is still to be explored, we investigated 4-azidopyridine (**1**) in regard of its capability of forming  $\text{SiCl}_4$  adducts (**2**) and the catalyst-free (3+2)-cycloaddition of **1** or **2** with phenylacetylene (Scheme 1).



**Scheme 1.** (a) Formation of adduct **2** from 4-azidopyridine (**1**) and  $\text{SiCl}_4$ . (b) (3+2)-cycloaddition of phenylacetylene and 4-azidopyridine. (c) Reaction of compound **2** and phenylacetylene.

## 2. Results and Discussion

### 2.1. Adduct Formation (4-Azidopyridine + $\text{SiCl}_4$ )

The reaction of 4-azidopyridine (**1**) and  $\text{SiCl}_4$  (in approximately 2:1 molar ratio) in chloroform at room temperature with stirring proceeded with the formation of a clear solution, from which a solid crystallized in the course of the following hours. This solid dissolved upon heating, and upon cooling, the product crystallized again. As both compound **1** and  $\text{SiCl}_4$  are liquids at room temperature, the solid state of the new product indicated the formation of an adduct (such as  $\text{SiCl}_4(4\text{-azidopyridine})_2$ ), and elemental analyses (C,H,N) were in accordance with this composition. Solution state NMR spectroscopy (of a sample dissolved in  $\text{CDCl}_3$ ), however, pointed at the co-existence of the starting materials. The  $^1\text{H}$  and  $^{13}\text{C}\{^1\text{H}\}$  spectra essentially represented those of **1**, and the  $^{29}\text{Si}\{^1\text{H}\}$  NMR spectrum exclusively exhibited a signal at ca.  $-19$  ppm, characteristic of  $\text{SiCl}_4$  with its tetracoordinate Si atom (cf. Appendix A incl. and Figure A1). Thus, dissolution and crystallization of this product proceed with dissociation and formation of the adduct  $\text{SiCl}_4(4\text{-azidopyridine})_2$ . In the course of exploring different crystallization conditions for improved yield, we noticed that both storage of the product solution at room temperature and in a fridge (ca.  $6$  °C) afforded a coarse-crystalline product (block-like crystals), whereas instant transfer of the solution into a freezer (ca.  $-39$  °C) gave rise to the formation of a fine-crystalline product with needle-shaped crystals. In both cases, crystals suitable for single-crystal X-ray diffraction analysis were found in the batches, and their analyses proved the formation of two different modifications of the product  $\text{SiCl}_4(4\text{-azidopyridine})_2$  (**2**) (Figures 2 and 3, Tables 1 and A1). Also, the crystallographic analyses confirmed the formation of the predicted Lewis acid-base adduct with a hexacoordinate Si atom. As the two crystalline modifications accommodate two different conformers of this compound, both the modifications and their respective conformers will be denoted as **2'** (for the variety obtained at a higher temperature) and **2''** (for the variety obtained at a lower temperature) in the following.

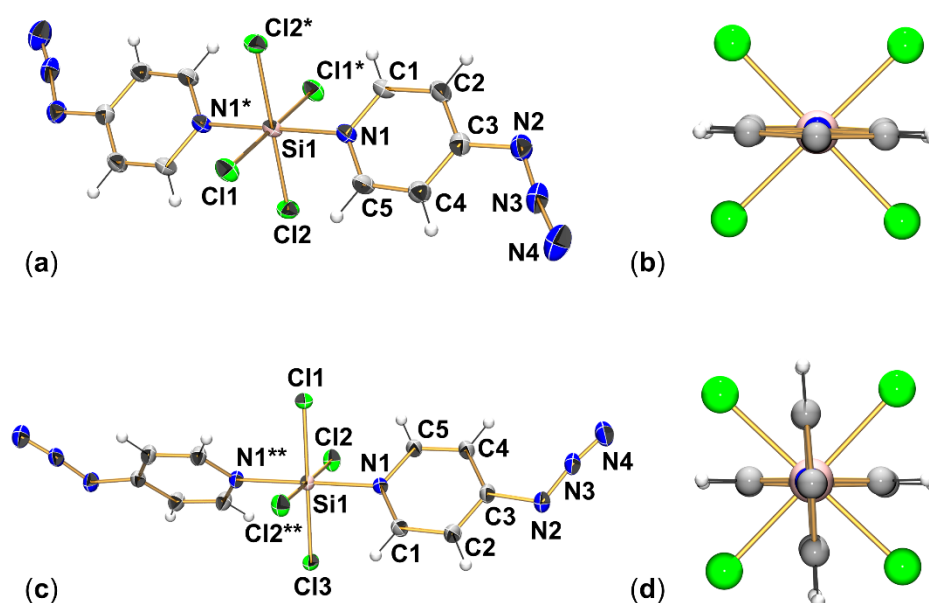


**Figure 2.** Molecular structure of (a)  $2'$  with displacement ellipsoids at the 50% probability level and labels of selected non-hydrogen atoms, supplemented by (b) a ball-and-stick model view along the N-Si-N axis of  $2'$  (with azido groups omitted for clarity). Sections (c) and (d) show the corresponding ellipsoid and ball-and-stick plots, respectively, for  $2''$ . The symmetry indicators \* and \*\* at some atom labels refer to the inversion at Si1 in  $2'$  ( $-x + 1, -y, -z + 1$ ) and the two-fold axis through Cl1-Si1-Cl3 in  $2''$  ( $-x, y, -z + 1/2$ ), respectively.

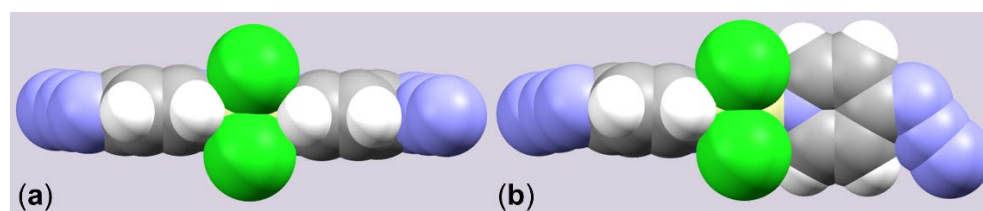


**Figure 3.** Space fill models of (a)  $2'$  and (b)  $2''$ .

**Table 1.** Selected bond lengths (Å) and angles (deg) of  $2'$  and  $2''$  in their crystal structures. (The symmetry indicators \* and \*\* at label N1 refer to the inversion at Si1 in  $2'$  ( $-x + 1, -y, -z + 1$ ) and the two-fold axis through Cl1-Si1-Cl3 in  $2''$  ( $-x, y, -z + 1/2$ ), respectively).

	$2'$	$2''$
Si1-Cl1	2.1859(5)	2.1895(7)
Si1-Cl2	2.1972(5)	2.1945(4)
Si1-Cl3		2.1904(7)
Si1-N1	1.9685(15)	1.9756(10)
C3-N2	1.405(2)	1.406(2)
N2-N3	1.257(3)	1.256(2)
N3-N4	1.123(3)	1.123(2)
N1-Si1-N1 */**	180	179.64(7)
C3-N2-N3	114.3(2)	116.1(2)
N2-N3-N4	173.4(2)	171.4(2)
C2-C3-N2-N3	177.6(2)	173.3(2)

In principle, both  $2'$  and  $2''$  feature octahedral *trans*-SiCl<sub>4</sub>N<sub>2</sub> coordination spheres, and their Si-Cl and Si-N bond lengths (Table 1) are similar to one another. Furthermore, these bonds are similar to those of the archetype complex SiCl<sub>4</sub>(pyridine)<sub>2</sub> [13], which exhibits Si-Cl and Si-N bond lengths of 2.183(4) and 1.976(9) Å, respectively. This allows the conclusion

that the 4-azido substituent (vs. H atom) has only marginal influence on the pyridine-N→Si coordination in the solid state. The azido groups themselves exhibit the same bond lengths in both crystal structures, but the C-N-N angle to and the N-N-N angle of the almost linear azido group as well as its variable torsion out of the pyridine plane (demonstrated by the C2-C3-N2-N3 dihedral angle) indicate its capability to adapt to different requirements of crystal packing. The influence of the packing on the N<sub>3</sub> moieties was probed with Raman spectroscopy. Both **2'** (at 2114 cm<sup>-1</sup>) and **2''** (at 2126 cm<sup>-1</sup>) give rise to absorption bands characteristic of the N<sub>3</sub> stretch mode (cf. bands at 2130 cm<sup>-1</sup> [36], at 2096 cm<sup>-1</sup> [37] and at 2135, 2093 cm<sup>-1</sup> [38] reported for the IR spectra of neat 4-azidopyridine). Whereas the overall appearance of the Raman spectra of **2'** and **2''** is very similar (cf. Figures S1 and S2 in the Supporting Information), this band of the N<sub>3</sub> stretch allows us to distinguish the two modifications. The difference in wave numbers (by 12 cm<sup>-1</sup>) must be attributed to various differences between the two modifications' azido groups' environments: In addition to the C-N-N angle and C-C-N-N torsion angle (cf. Table 1), the N<sub>3</sub> groups are involved in different H contacts. In **2'**, a close contact is found at N2 (C2\*-H2\*...N2, \* = symmetry equivalents according to 2 - x, 1 - y, 1 - z) with N-H and N-C distances of 2.61 Å and 3.55 Å, respectively, and a C-H-N angle of 169°. In contrast, in **2''** the closest H contacts at the N<sub>3</sub> group are found at N4 (C5\*-H5\*...N4, \* = x + 0.5, 0.5 - y, z + 0.5; N-H 2.74 Å, N-C 3.67 Å, C-H-N 167°; C4\*\*-H4\*\*...N4, \*\* = 2 - x, 0.5 - y, 1 - z; N-H 2.77 Å, N-C 3.63 Å, C-H-N 150°). In addition, the azido groups are involved in close Cl1...N3\*\*\* and Cl1...N3\*\*\*\* contacts, \*\*\* = x - 1, 0.5 - y, 1 - z, \*\*\*\* = x - 0.5, 0.5 - y, z - 0.5, Cl-N 3.20 Å. Note: For these contacts, no s.u.s are given because they are below 0.01 for the non-H-atom separations, and the H atom positions have not been refined (positioning of H atoms in the structure model in idealized positions).

In both modifications **2'** and **2''**, the Si atoms of the silicon complexes are located in a special position (in **2'** on a center of inversion, in **2''** on a two-fold axis), which also has the consequence that the asymmetric unit is constituted by a half molecule of this complex in each case. Whereas in the former, the crystallographic symmetry element implies a constraint on the N-Si-N angle of 180° (and parallel arrangement of the pyridine rings), the latter liberates this parameter. Nonetheless, also in **2''**, the N-Si-N angle is close to 180°. The space fill model in Figure 3 demonstrates that the N-Si-N coordination is also stabilized by two bifurcated Cl...H...Cl contacts between the pyridine H atoms in 2,6-position and Cl atoms of two alternating quadrants of the square-shaped SiCl<sub>4</sub> plane. These interactions on the two opposite sides of the SiCl<sub>4</sub> plane stabilize the N→Si coordination perpendicular to the SiCl<sub>4</sub> plane and thus the essentially linear angle. The striking difference between **2'** and **2''**, however, is the dihedral angle between the pyridine planes (ca. 0° and ca. 90°, respectively). In **2'**, the opposing pyridine H atoms establish bifurcated Cl...H...Cl contacts within the same quadrants of the SiCl<sub>4</sub> plane (we may call it an eclipsed conformation), whereas in **2''** the quadrants are alternating (in a staggered conformation). Interestingly, inspection of the crystallographically characterized silicon tetrahalide pyridine adducts available in the Cambridge Structure Database (a search in CSD 2023 version 5.44) revealed the exclusive encountering of the eclipsed conformation. In SiCl<sub>4</sub>(pyridine)<sub>2</sub> [13], which is located on a crystallographically imposed bisecting plane (in space group C2/m), the pyridine rings are forced to coplanarity and, because of near square-planar SiCl<sub>4</sub>-arrangement, C-N-Si-Cl torsion angles must be close to 45°, but even in case of crystal structures devoid of the mirror symmetry these torsion angles are close to 45° (in **2'** they are in the range 44.3(2)°–46.9(1)°), and the C-N-N-C torsion angles are merely 2.1(3)°. Even though in complex SiF<sub>4</sub>(4-phenylpyridine)<sub>2</sub> [12] the dihedral angle between the pyridine planes deviates markedly from 0° (C-N-N-C torsion angles are 34.9(3)° and 35.9(3)°, and C-N-Si-F torsion angles of 26.7(4)° and 27.4(4)° are encountered) the F...H contacts of opposing pyridine ligands are still within the same quadrants of the SiF<sub>4</sub> plane. As an isolated example, only in the case of SiCl<sub>2</sub>H<sub>2</sub> complexes, where the dihedral angle of pyridines deviates markedly from planarity in SiCl<sub>2</sub>H<sub>2</sub>(4-ethylpyridine)<sub>2</sub> (C-N-N-C torsion angles are 39.1(1)° and 41.4(1)°) [17], the pyridine 2,6-H-atoms of opposing pyridine ligands are pointing into



alternating quadrants of the  $\text{SiCl}_2\text{H}_2$  plane (with C-N-Si-H torsion angles of  $19.5(1)^\circ$  and  $20.7(1)^\circ$ ). Figure 4 gives a schematic impression of the conformations encountered with most of the  $\text{Si}(\text{halide})_4(\text{pyridine})_2$  complexes (e.g., in the parent complex  $\text{SiCl}_4(\text{pyridine})_2$  [13]), as well as with  $\text{SiF}_4(4\text{-phenylpyridine})_2$  [12],  $\text{SiCl}_2\text{H}_2(4\text{-ethylpyridine})_2$  [17] and the ultimate staggered conformation in  $2''$ . The latter features C-N-N-C torsion angles of  $85.0(1)^\circ$  and  $88.3(1)^\circ$ , as well as C-N-Si-Cl torsion angles in the range of  $42.6(1)^\circ$ – $47.9(1)^\circ$ . This exposes  $2''$  as the first example of a real staggered conformation within the class of octahedral pyridine–silane adducts. As the intramolecular interactions (one N→Si dative bond and two  $\text{Cl}\cdots\text{H}\cdots\text{Cl}$  contacts per pyridine ligand) are essentially the same in both conformers  $2'$  and  $2''$ , we analyzed the energetic difference between the two varieties (conformers and modifications) with the aid of computational methods to find an answer as to why the eclipsed conformation may dominate the crystallographically encountered molecular shapes.

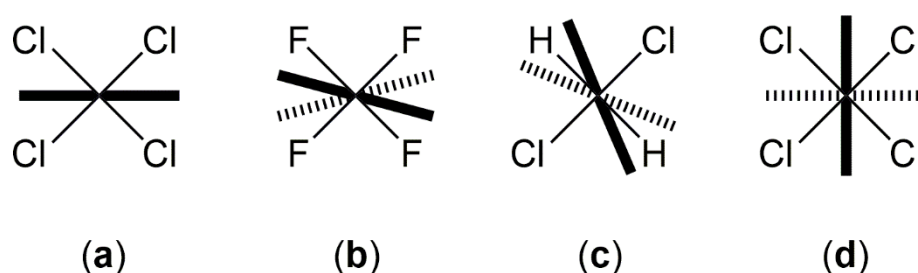


**Figure 4.** Schematic representation of the conformations of Si-coordinated pyridine moieties (view along the idealized N-Si-N axis, the bold and dashed lines represent the planes of the pyridine ligands in the front and back, respectively) of (a)  $2'$  and various other  $\text{Si}(\text{halide})_4(\text{pyridine})_2$  complexes (such as  $\text{SiCl}_4(\text{pyridine})_2$  [13]), (b)  $\text{SiF}_4(4\text{-phenylpyridine})_2$  [12], (c)  $\text{SiCl}_2\text{H}_2(4\text{-ethylpyridine})_2$  [17] and (d)  $2''$ .

For the isolated molecule of compound **2**, a Potential Energy Surface Scan (PES) was performed for the rotation of one pyridine ring about the N-Si-N axis (variation in the C-N-N-C dihedral angle in increments of  $10^\circ$  followed by partial relaxation of the remaining parameters, starting from the fully optimized molecular structure of  $2'$ ). Close to local minima, full optimization was allowed for analysis of the local energetic minimum. The diagram in Figure 5 shows the energetic development of the conformational variation for a  $180^\circ$  rotation. In addition to the conformations at  $0^\circ$  and  $180^\circ$  (which are basically distinguished by their relative orientations of the remote azido groups), the conformation at a dihedral angle of  $90^\circ$  (staggered conformation corresponding to  $2''$ ) exhibits an energetic minimum of essentially the same depth (the energetic difference of  $0.13 \text{ kcal mol}^{-1}$  can be interpreted as meaningless). This is in accordance with an older study of  $D_{2h}$  and  $D_{2d}$  symmetric conformers of *trans*- $\text{SiCl}_4(\text{pyridine})_2$ . These conformers were shown to exhibit essentially the same thermodynamic characteristics (enthalpy and entropy of dissociation into  $\text{SiCl}_4$  and pyridine) [39]. Thus, the packing efficiency might be the predominant parameter. Analysis of the Hirshfeld surface (HS) of  $2'$  indicates a greater number and higher intensity of close intermolecular contacts with respect to the HS of  $2''$  (Appendix C, Figures A2–A4). For an energetic analysis of the difference in packing, DFT methods were applied. The molecules of  $2'$  and  $2''$  were optimized in their periodic crystal environment (with full optimization of the molecular conformation and optimization of the unit cell parameters allowed, as the analysis aimed at an energetic comparison at 293 K rather than a comparison at the temperature of crystal structure determination (which was 200 K). The analysis revealed  $2'$  in its crystal environment to be more stable than  $2''$  in its packing by  $8.5 \text{ kcal mol}^{-1}$  with respect to 1 mol of each kind of molecule in its respective crystal environment. In regard to the experimental data, this computational finding is in accordance with the different molecular volumes occupied in their crystal packings:

Whereas in **2''** one molecule of the complex requires a volume of  $416 \text{ \AA}^3$ , the volume per molecule of  $393 \text{ \AA}^3$  indicates a much more efficient packing for **2'**.

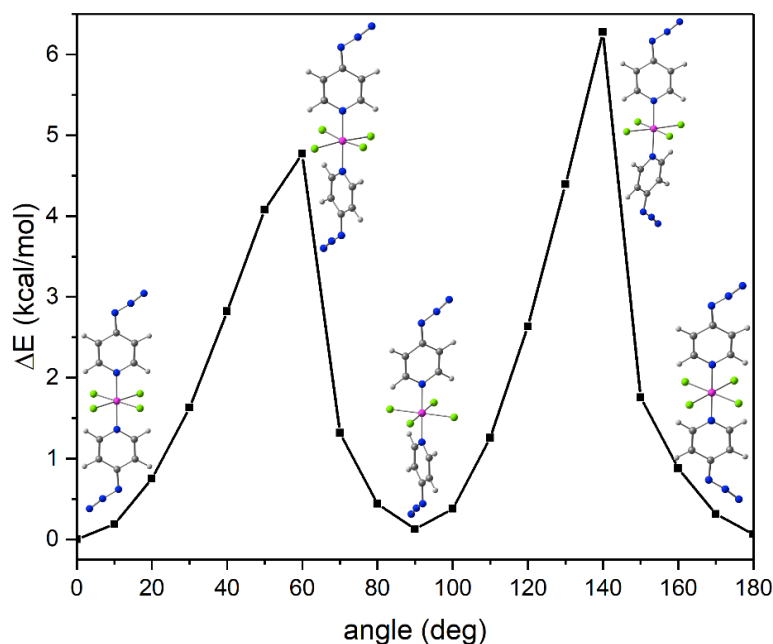


**Figure 5.** Energetic development of a Potential Energy Surface Scan (PES) for the torsion of a pyridine ligand about the N-Si-N axis in increments of  $10^\circ$  (followed by partial relaxation), starting from the molecular conformation of **2'**.

From the above results, we can conclude that conformers **2'** and **2''** (as isolated molecules in chloroform solvent environment) should coexist in solution. However, **2'** (in its crystalline arrangement) represents the thermodynamically more favored modification, and **2''** (in its crystalline form) must be a result of kinetics. Apparently, the arrangement of **2''** in the solid allows for easier crystal seed formation upon cooling, thus enabling isolation of crystalline **2''** by crystallization at  $-39^\circ\text{C}$ , whereas crystallization at room temperature either inhibits the formation of seeds of **2''** or causes their rapid dissolution and eventually yields crystals of the more stable modification and conformer **2'**.

In addition to the crystallization at low temperatures, the accessibility of **2''** depends on the solvent used. Syntheses of **2** in toluene, both by gas phase diffusion of  $\text{SiCl}_4$  into a toluene solution of **1** at room temperature and by adding **1** to a toluene solution of  $\text{SiCl}_4$  at  $-78^\circ\text{C}$  with stirring, resulted in the formation of **2'**. In the former case, large crystals were obtained, and the determination of the unit cell confirmed the presence of modification **2'**. In the latter case, a fine powder was obtained, and  $^{13}\text{C}$  CP/MAS NMR spectroscopy thereof confirmed the formation of **2'** (vide infra).

The availability of the two conformers **2'** and **2''** in their solid forms allowed for comparative investigation of their  $^{13}\text{C}$  and  $^{29}\text{Si}$  NMR properties in the solid state. Each of the  $^{13}\text{C}$  NMR spectra (Figure 6) features five signals, a pattern which is in accordance with the five crystallographically independent pyridine C atoms in each of the crystal structures **2'** and **2''**. Each of the two spectra exhibits two signals of the rather well-shielded C atoms in 3,5-position of the pyridine ring as well as three noticeably more downfield located signals for the C atoms in 2,6- and 4-position, the latter being the most downfield shifted signal. (The assignment of the latter  $^{13}\text{C}$  NMR signal to the 4-position was made by cross-polarization magic angle spinning (CP/MAS) spectra of variable CP contact times. Whereas contact times of  $\tau = 2 \text{ ms}$  were sufficient for polarization transfer to all different kinds of  $^{13}\text{C}$  atoms, noticeably shorter contact times ( $\tau = 100 \text{ }\mu\text{s}$ ) only allowed for efficient polarization transfer to the  $^{13}\text{C}$  sites involved in a C-H bond.) The absence of the signals of **2'** in the spectrum of **2''** (and vice versa) indicates the clear predominance of each of the

crystalline modifications in the respective sample. The latter finding is essential for the evaluation of the  $^{29}\text{Si}$  solid-state NMR spectra (Figure 7). In spite of the different molecular conformations,  $2'$  ( $\delta_{\text{iso}} = -177.4$ ) and  $2''$  ( $\delta_{\text{iso}} = -177.8$ ) exhibit practically the same isotropic  $^{29}\text{Si}$  NMR shift in the solid state and, as a consequence, the spinning side bands are located in corresponding positions for spectra recorded at the same MAS frequency. Determination of the principal values of the chemical shift anisotropy (CSA) tensor from the spinning side band spectra relies on the prerequisite that the side band pattern is produced by nuclei with one CSA tensor rather than being a superposition of two different side band spectra in unknown ratio. The CSA tensor data extracted from the spectra in Figure 7a,b are listed in Table 2. These data are complemented by the corresponding values calculated for the molecules of  $2'$  and  $2''$  (the atomic coordinates of which had been optimized in their crystal environment, and referencing of their calculated  $^{29}\text{Si}$  NMR shifts was performed with tetramethylsilane as well as with  $\text{SiCl}_2(\text{oxinate})_2$  [40]).

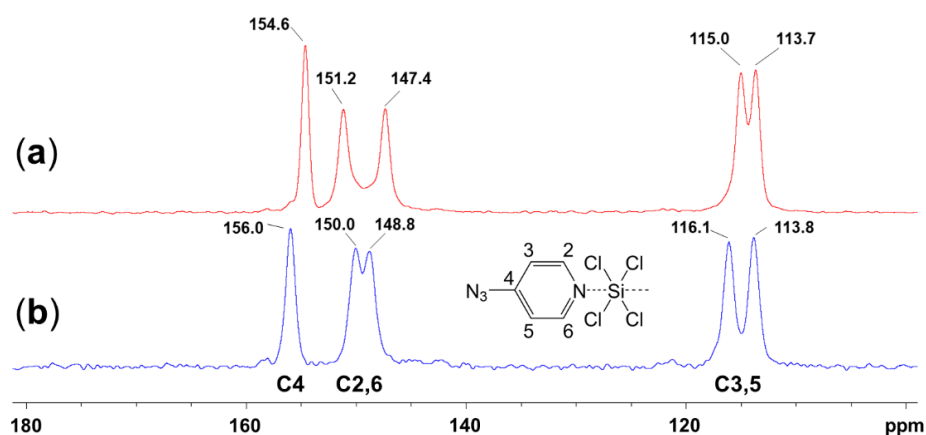


**Figure 6.**  $^{13}\text{C}$  CP/MAS NMR spectra of (a)  $2''$  and (b)  $2'$  recorded at a MAS frequency of 10 kHz and with a CP contact time of  $\tau = 2$  ms. The graphic shows the signals at the isotropic chemical shifts with signal assignment. (In accordance with the crystal structures, cf. Figure 2, in both solids, the C atom positions 2,6 as well as 3,5 are chemically not equivalent).

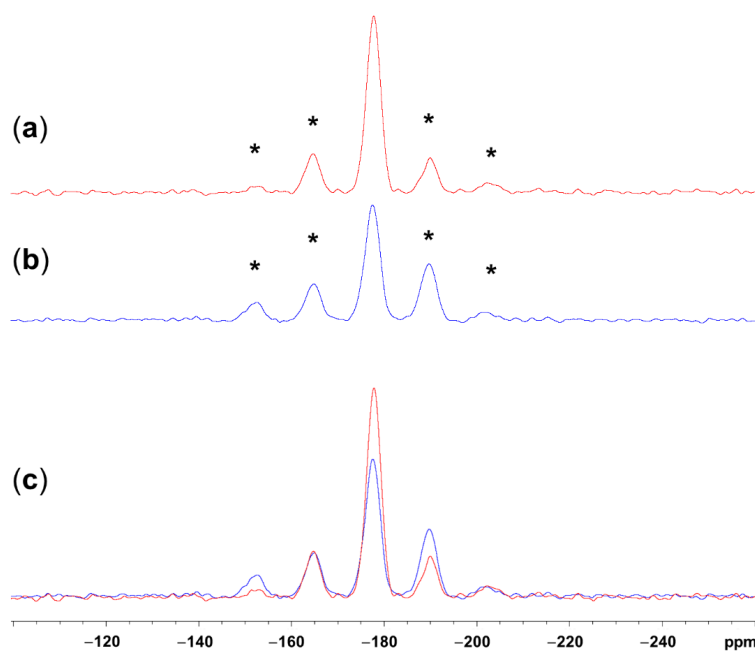


**Figure 7.**  $^{29}\text{Si}$  CP/MAS NMR spectra of (a)  $2''$ , (b)  $2'$ , and (c) an overlay of both spectra, recorded at



an MAS frequency of 1 kHz. The spinning side bands are marked with an asterisk (\*). In the overlay (c), the intensities of the two spectra were adjusted to the side band at  $-165$  ppm, which has a similar relative intensity in both spectra (in both cases, its integral represents ca. 15% of the sum of integrals of the isotropic signal and the two adjacent side bands).

**Table 2.**  $^{29}\text{Si}$  CSA tensor characteristics (isotropic chemical shift  $\delta_{\text{iso}}$ , principal components  $\delta_{11}$ ,  $\delta_{22}$ ,  $\delta_{33}$ , span  $\Omega$  and skew  $\kappa$ ) of  $2'$  and  $2''$  determined from solid-state NMR spectra (cf. Figure 7) as indicated with suffix (exp) as well as the corresponding data calculated for these molecules upon optimization of their atomic coordinates in the crystal environment, indicated with suffix (calc-ref1) for referencing against the isotropic chemical shift calculated for tetramethylsilane (TMS) set at  $\delta = 0$  ppm, and with suffix (calc-ref2) for referencing against the isotropic chemical shift calculated for the optimized molecular structure of  $\text{SiCl}_2(\text{oxinate})_2$  in its crystal structure set at  $\delta = -158.7$  ppm [40]. The entries  $2'$  (calc-ref1-0°opt) and  $2''$  (calc-ref1-90°opt) contain the corresponding CSA tensor characteristics calculated for the eclipsed and staggered, respectively, local minimum molecular conformation of  $2'$  and  $2''$  (cf. entries at 0° and 90°, respectively, in Figure 5) upon full optimization of the molecular conformation in chloroform solvent environment (COSMO model) and referenced against TMS.

Compound	$\delta_{\text{iso}}$	$\delta_{11}$	$\delta_{22}$	$\delta_{33}$	$\Omega$	$\kappa$
$2'$ (exp)	-177.4	-150.7	-184.2	-197.2	46.5	-0.44
$2'$ (calc-ref1)	-167.6	-141.7	-176.3	-184.8	45.6	-0.60
$2'$ (calc-ref2)	-171.9	-146.0	-180.6	-189.1	45.6	-0.60
$2'$ (calc-ref1-0°opt)	-174.9	-144.8	-185.7	-194.1	49.3	-0.66
$2''$ (exp)	-177.8	-161.0	-175.3	-197.0	36.0	+0.21
$2''$ (calc-ref1)	-168.3	-154.3	-167.8	-182.8	28.5	+0.05
$2''$ (calc-ref2)	-172.6	-158.6	-172.1	-187.1	28.5	+0.05
$2''$ (calc-ref1-90°opt)	-174.5	-163.5	-163.7	-196.4	32.9	+0.98

The features of the CSA tensors (the order of the principal components  $\delta_{11}$ ,  $\delta_{22}$ , and  $\delta_{33}$ , as well as span  $\Omega$  and skew  $\kappa$ ) are reported according to the Herzfeld–Berger notation [41,42]. The calculated CSA tensors represent the features of the experimentally determined data of the two modifications  $2'$  and  $2''$  very well, especially the narrow span (with its feature  $\Omega(2') > \Omega(2'')$ ) and the noticeable difference in the skew are reflected effectively. With respect to the chemical shift scale, however, the calculated data are systematically downfield shifted. This may, in part, originate from referencing data calculated for compounds optimized in crystal environment against data calculated for an isolated molecule, TMS (cf. entries calc-ref1). Therefore, the molecule  $\text{SiCl}_2(\text{oxinate})_2$  [40] was employed as an alternative reference for this calculation (cf. entries calc-ref2). In addition to being a solid, this compound features hexacoordinate Si, as well as some N and Cl atoms, in its coordination sphere. This approach improved the fit of the CSA tensor on the chemical shift scale to some extent. For both  $2'$  and  $2''$ , the greatest deviations between experimental and calculated CSA tensors are found for principal component  $\delta_{33}$ , which points along the N-Si-N axis. The orientations of the CSA principal components within the molecules are visualized in Figures S14 and S15 in the Supporting Information. With respect to CSA tensors of related pyridine adducts (“pyridine” may represent a variety of 4-substituted pyridines) of dichlorosilane [17] and trichlorosilane [19], the isotropic chemical shifts of the  $\text{SiCl}_4$  adducts  $2'$  and  $2''$  are more upfield, which reflects a trend  $\delta_{\text{iso}}(\text{SiCl}_2\text{H}_2(\text{“pyridine”})_2) > \delta_{\text{iso}}(\text{SiCl}_3\text{H}(\text{“pyridine”})_2) > \delta_{\text{iso}}(\text{SiCl}_4(\text{“pyridine”})_2)$ . For both the pyridine adducts of dichlorosilane [17] and trichlorosilane [19], the most shielded direction was shown to point along the N-Si-N axis, with CSA tensor principal values  $\delta_{33}$  of ca.  $-200$  ppm (e.g.,  $-210$  ppm for  $\text{SiCl}_2\text{H}_2(4\text{-}t\text{Bu-pyridine})_2$  [17] and  $-202$  ppm for  $\text{SiCl}_3\text{H}(4\text{-}t\text{Bu-pyridine})_2$  [19]). This feature is reflected by compounds  $2'$  and  $2''$ , both of which exhibit very similar values for  $\delta_{33}$  ( $-197$  ppm) and imply a trend of decreasing shielding in this direction with an increase in Cl (instead of H) substitution at the Si atom. Principal axes (11) and (22), which are located in the  $\text{SiCl}_4$  plane, are influenced by the

different relative conformations of the pyridine ligands. Whereas in **2'** the pyridine rings are nearly coplanar and thus can exert simultaneous in-plane and perpendicular-to-plane shielding effects, the angular dependence of the shielding in **2''** is always determined by both kinds of effects because of the torsion of the pyridine rings, causing an approaching of  $\delta_{11}$  and  $\delta_{22}$  to one another. The upfield shift of principal value  $\delta_{11}$  (by ca. 10 ppm), which results therefrom, can be seen as the major cause of the reduced span  $\Omega$  (by ca. 10 ppm) for the CSA tensor of **2''**. (This is also reflected by the graphic in Figure S16.) Moreover, the mutual approaching of  $\delta_{11}$  and  $\delta_{22}$  to one another eventually causes a noticeable change in the skew  $\kappa$ . This is furthermore supported by the CSA tensor characteristics calculated for the optimized conformer of  $\text{SiCl}_4(4\text{-azidopyridine})_2$  at a dihedral angle of  $90^\circ$  between the pyridine ligands (cf. the conformation, which represents the local minimum at  $90^\circ$  of the PES analysis in Figure 5). Entry **2''** (calc-ref1- $90^\circ$ opt) in Table 2 shows that this closer approach to a  $D_{2d}$  symmetric conformer (merely the remote  $\text{N}_3$  groups violate this symmetry) should eventually result in an axial CSA tensor with identical values for  $\delta_{11}$  and  $\delta_{22}$  as well as a skew  $\kappa = 1$  resulting therefrom.

## 2.2. Click Reaction of 4-Azidopyridine and Phenylacetylene

The azido group, which has been a spectator substituent only in Section 2.1., offers an intriguing entry into further chemistry. Whereas the decomposition of azides with formation of nitrenes opens various routes of further syntheses [43,44], the intact azido group can be utilized in (3+2)-cycloadditions with unsaturated groups such as alkynes [45–47] or nitriles [48]. As nitriles may represent competitor Lewis bases (some examples of complexes of pronounced Lewis acidic silanes and nitrile ligands even allowed for their crystallographic investigation [22,49,50]), we chose an alkyne (i.e., phenylacetylene) to investigate its (3+2)-cycloaddition with 4-azidopyridine and with the  $\text{SiCl}_4$  adduct thereof. (3+2)-cycloadditions of azides and alkynes are facile, especially when carried out in protic solvents (e.g., in *t*BuOH/water [46]) and when catalyzed by transition metals or some of their complexes [51]) which contributed to their classification as “Click reactions”. Aiming at investigations of related cycloadditions of alkynes and silicon complexes such as **2**, it is clear that both protic solvents and transition metal catalysts need to be avoided. The former likely cause solvolysis of, e.g., Si–Cl bonds and the latter may bind to the pyridine ligand and thus compete with Si complex formation. Thus, we explored the thermal addition of 4-azidopyridine and phenylacetylene in rather innocent hydrocarbyl solvents (toluene and *p*-xylene). Upon cooling to room temperature, the reaction products crystallized because of the poor solubility in the solvents used. Both isomers, the 1,4- and the 1,5-substituted triazole **1,4-3** and **1,5-3**, respectively, formed, as indicated in Scheme 1. The total weight of the isolated product provided information on the degree of conversion, and the different crystal shapes (**1,4-3** formed thin plates, **1,5-3** formed compact blocks) allowed for crystal picking and, thus, for the determination of their individual crystal structures by single-crystal X-ray diffraction (Table A1, Figure A5). With respect to the latter, graphics of the molecules (Figures S8 and S9) and tables with selected bond lengths and angles (Tables S1 and S2) are provided in the Supporting Information. Furthermore, we point out that the structure of **1,5-3** (with respect to the unit cell parameters) is related to that of 4-phenyl-3-(4-pyridyl)-4H-1,2,4-triazole [52], which also has essentially the same molecular shape as compound **1,5-3**. The structure of **1,4-3** is related to that of 3,6-bis(pyridin-4-yl)pyridazine [53]. These molecules also have similar molecular shapes. However, in this case, they share a similar reduced unit cell only (**1,4-3** crystallized in a triclinic cell, the latter in the monoclinic space group type  $C2/c$ , which is possible because of the higher symmetry of the molecule). NMR spectroscopic data of these two isomers are available in the literature [54]. They allowed for signal assignment in the spectra of the samples obtained and for the determination of the isomer ratio by integration of selected  $^1\text{H}$  NMR signals. For that purpose, the samples obtained along the series of varied solvents and reaction times were finely ground before a representative sample was dissolved in  $\text{CDCl}_3$  for  $^1\text{H}$  NMR spectroscopic determination of the isomer ratio. Table 3 contains the

results of that series. In principle, in this solvent environment and in the absence of any catalyst, the (3+2)-cycloaddition of 4-azidopyridine and phenylacetylene is rather slow and proceeds in the course of some hours at temperatures above 100 °C. As expected, the reaction rate is enhanced by elevated temperatures (reflux temperature of p-xylene rather than toluene). The ratio of isomers in the isolated product, however, is hardly altered. The isomer ratio was determined from the ratio of  $^1\text{H}$  NMR signal integrals of the protons shown in Figure 8.

**Table 3.** Results of (3+2)-cycloaddition reactions of **1** and excess phenylacetylene (4.6 mmol) in 5 mL of the respective solvent.

Solvent	<i>n</i> ( <b>1</b> ) (mmol)	<i>T</i> (°C)	<i>t</i> (h)	Yield <sup>1</sup> (mmol)	Yield <sup>1</sup> (%)	%(1,4-3)	%(1,5-3)
Toluene	3.5	110	0.5	0.74	21	29	71
Toluene	3.9	110	2.0	1.63	42	30	70
p-Xylene	3.4	140	0.5	1.41	42	31	69
p-Xylene	3.2	140	2.0	2.01	76	33	67

<sup>1</sup> The yield reported in this table is the yield of the solid product obtained upon storage of the reaction mixture for one day at room temperature.

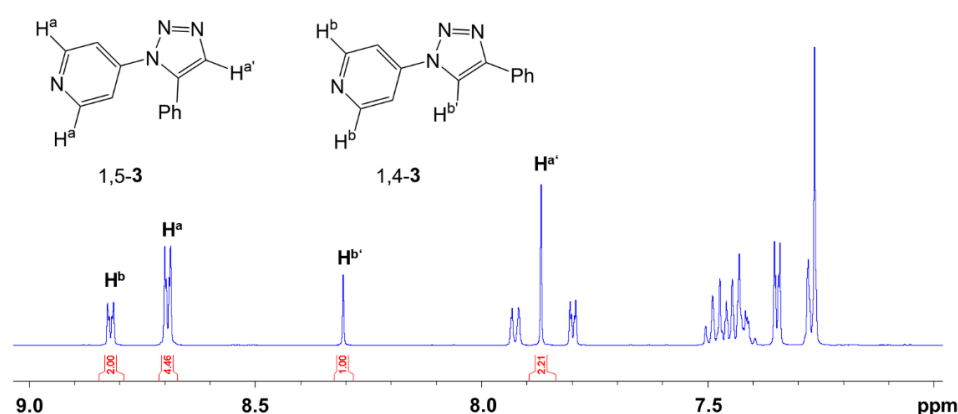


**Figure 8.**  $^1\text{H}$  NMR signals of the mixture of 1,4-3 and 1,5-3 obtained by reaction of 4-azidopyridine and phenylacetylene in p-xylene at 140 °C for 0.5 h (with signals used for determination of isomer ratio and a sketch with a signal assignment to the protons of origin).

As compound **2** exhibits very poor solubility in toluene and p-xylene, we probed the (3+2)-cycloaddition of **1** and phenylacetylene as well as the related reaction of **2** and phenylacetylene in chloroform at 60 °C (Table 4). For the purpose of  $^1\text{H}$  NMR spectroscopic analysis of the resultant solution,  $\text{CDCl}_3$  was used. The relevant parts of the  $^1\text{H}$  NMR spectra, which were used for the evaluation of the results, are shown in Figure 9. Entries 1 and 2 of Table 4 (spectra (a) and (b), respectively, in Figure 9) contain the results of  $\text{CDCl}_3$  solutions of comparable molar concentrations of 4-azidopyridine moieties and phenylacetylene. In spite of the slightly higher concentration of starting materials for entry 2, the conversion is merely one-third with respect to the same reaction carried out with a solution of the  $\text{SiCl}_4$  adduct **2**. Furthermore, the presence of  $\text{SiCl}_4$  in the solution (entry 1) enhances the selectivity of the (3+2)-cycloaddition in favor of triazole isomer 1,5-3 (an isomer ratio 1,4-3:1,5-3 of ca. 1:6 was encountered). Higher concentrations of starting materials (**1** and phenylacetylene, cf. Table 4 entry 3) may enhance the conversion of the reaction within this time frame, but the product ratio (ca. 1:3) remains essentially the same and, furthermore, rather similar to the (1:2)-ratio observed for this non-catalyzed reaction when performed in toluene or p-xylene (cf. Table 3).

**Table 4.** Results of (3+2)-cycloaddition reactions of **1** or **2** and phenylacetylene in CDCl<sub>3</sub> (4 h at 60 °C).

Entry	V(CDCl <sub>3</sub> ) (mL)	-N <sub>3</sub> Source	<i>n,m</i> (-N <sub>3</sub> Source) (mmol, mg)	<i>n,m</i> (PhCCH) (mmol, mg)	Conversion (%)	%(1,4-3)	%(1,5-3)
1	2.8	<b>2'</b>	0.34, 139	0.71, 73	1.85	14	86
2	2.8	<b>1</b>	0.77, 93	0.78, 80	0.62	26	74
3	3.8	<b>1</b>	3.46, 415	3.43, 350	1.90	25	75

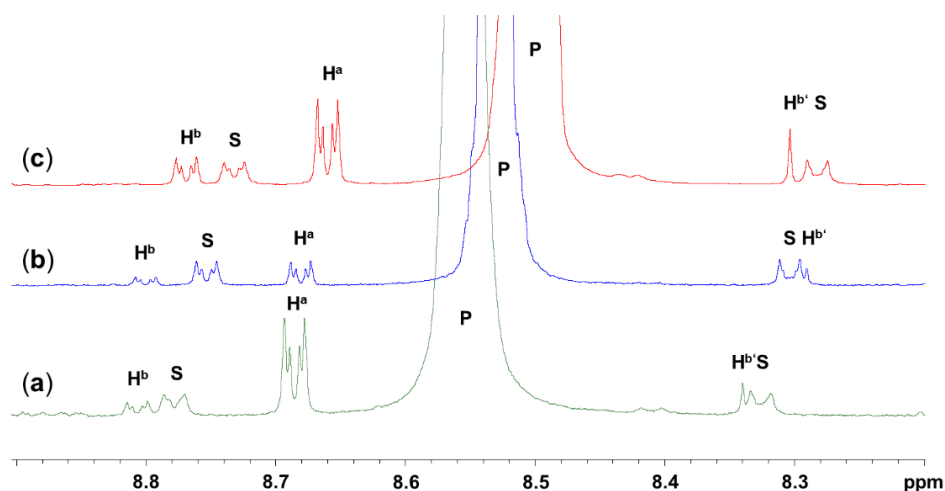


**Figure 9.** Selected section of the <sup>1</sup>H NMR spectra used for determination of the data shown in Table 4. Subfigures (a), (b), and (c) correspond to entries 1, 2, and 3, respectively, in Table 4. The signal assignments H<sup>a</sup> and H<sup>b</sup> (as well as H<sup>b'</sup>) are the same as in Figure 8. The additional signals, denoted with P and S, are the parent signals of the 2,6 protons of remaining starting material 4-azidopyridine and their <sup>1</sup>J(<sup>13</sup>C<sup>1</sup>H) satellites, respectively. Because of the severe superposition of signal H<sup>b'</sup> with satellites, signals H<sup>a</sup> and H<sup>b</sup> were used for the determination of the isomer ratio. The slightly different individual chemical shifts are attributed to their dependence on the concentration of the various species in the solution (e.g., solvent, 4-azidopyridine, phenylacetylene) and on the presence vs. absence of SiCl<sub>4</sub> in these solutions.

### 3. Materials and Methods

#### 3.1. General Considerations

**Caution:** Some azides may be highly explosive, and safety precautions were taken for the preparation of organic azides such as 4-azidopyridine [38]. Therefore, in addition to precautions such as working behind a blast shield and preparation of 4-azidopyridine in an apparatus open to the atmosphere, avoiding direct sunlight and contact with metals, the preparation of this starting material was limited to the 5 g scale. Furthermore, even though we did not encounter any hints at the hazardous explosive nature of SiCl<sub>4</sub> adducts of 4-azidopyridine, we applied similar precautions (albeit working under an inert atmosphere) for the further conversions of this compound, too. In the case of solid reaction products (such as **2**), excessive heating of the pure compound or of the undissolved solid in dispersions was avoided.

Starting materials SiCl<sub>4</sub> (ABCR, Karlsruhe, Germany, 98%), 4-chloropyridine hydrochloride (Sigma-Aldrich, St. Louis, MO, USA, 99%), and sodium azide (AppliChem, Darmstadt, Germany, pure) were used as received without further purification. Phenylacetylene (Fluka, Buchs, Switzerland, 97%) was distilled and stored in a fridge prior to use. 4-Azidopyridine [38] was prepared according to a literature method. Toluene was dried using an MBraun SPS-800 setup (MBraun, Garching, Germany). p-Xylene (Sigma-Aldrich, Steinheim, Germany, >98%), chloroform, stabilized with amylenes (Honeywell, Seelze, Germany, ≥99.5%) and CDCl<sub>3</sub> (Deutero, Kastellaun, Germany, 99.8%) were stored over

activated molecular sieves (3 Å) for at least 7 days and used without further purification. All reactions that involved  $\text{SiCl}_4$  or the 4-azidopyridine adducts thereof, as well as the reactions of 4-azidopyridine and phenylacetylene, were carried out under an atmosphere of dry argon utilizing standard Schlenk techniques. Solution NMR spectra ( $^1\text{H}$ ,  $^{13}\text{C}$ ,  $^{29}\text{Si}$ ) (cf. Figures S3–S5 in the Supporting Information) were recorded on Bruker Avance III 500 MHz and Bruker Nanobay 400 MHz spectrometers.  $^1\text{H}$ ,  $^{13}\text{C}$  and  $^{29}\text{Si}$  chemical shifts are reported relative to  $\text{Me}_4\text{Si}$  (0 ppm) as internal reference.  $^{29}\text{Si}$  and  $^{13}\text{C}$  CP/MAS NMR spectra (cf. Figures S6 and S7 in the Supporting Information) were recorded on a Bruker Avance 400 WB spectrometer using 4 mm zirconia ( $\text{ZrO}_2$ ) rotors (in some cases in combination with KelF-inserts) and a MAS frequency of  $\nu_{\text{rot}} = 1$  kHz and 10 kHz for  $^{29}\text{Si}$  and  $^{13}\text{C}$ , respectively. ( $^{29}\text{Si}$   $\delta_{\text{iso}}$  values were determined at  $\nu_{\text{rot}} = 3$  kHz.) The chemical shift is reported relative to  $\text{Me}_4\text{Si}$  (0 ppm) and was referenced externally for  $^{29}\text{Si}$  to octakis(trimethylsilyloxy)octasilsesquioxane  $\text{Q}_8\text{M}_8$  (most upfield signal of  $\text{Q}^4$  groups at  $\delta_{\text{iso}} = -109$  ppm) and for  $^{13}\text{C}$  to adamantane (downfield signal, at  $\delta_{\text{iso}} = 38.5$  ppm). Determination of CSA tensor principal values from the spinning side bands in the  $^{29}\text{Si}$  CP/MAS NMR spectra was performed with DMFIT [55]. Raman spectra (cf. Figures S1 and S2 in the Supporting Information) were measured with a Bruker FT-Raman spectrometer RFS 100/S (Bruker Optics, Ettlingen, Germany). The device works with an air-cooled Nd:YAG-Laser with a wavelength of 1064 nm and a nitrogen-cooled detector. Elemental analyses were performed on an Elementar Vario MICRO cube. For single-crystal X-ray diffraction analyses, crystals were selected under an inert oil and mounted on a glass capillary (which was coated with silicone grease). Diffraction data were collected on a Stoe IPDS-2/2T diffractometer (STOE, Darmstadt, Germany) using Mo  $\text{K}\alpha$ -radiation. Data integration and absorption correction were performed with the STOE software XArea and XShape, respectively. The structures were solved via direct methods using SHELXS or SHELXT and refined with the full-matrix least-squares methods of  $F^2$  against all reflections with SHELXL-2018/3 or SHELXL-2019/3 [56–60]. All non-hydrogen atoms were anisotropically refined, and hydrogen atoms were isotropically refined in idealized positions (riding model). For details of data collection and refinement, see Appendix B, Table A1. Graphics of molecular structures were generated with ORTEP-3 [61,62], POV-Ray 3.7 [63], and MERCURY [64]. CCDC 2302622 (**2'**), 2302624 (**2''**), 2302625 (**1,4-3**) and 2302623 (**1,5-3**) contain the supplementary crystal data for this article. These data can be obtained free of charge from the Cambridge Crystallographic Data Centre via <https://www.ccdc.cam.ac.uk/structures/> (accessed on 21 October 2023).

The geometry optimizations of isolated molecules were carried out with ORCA 5.0.3 [65] using the restricted PBE0 functional with a relativistically recontracted Karlsruhe basis set ZORA-def2-TZVPP [66,67] for all atoms, scalar relativistic ZORA Hamiltonian [68,69], atom-pairwise dispersion correction with the Becke–Johnson damping scheme (D3BJ) [70,71] and COSMO solvation (chloroform). Calculations were started from the molecular structures obtained by single-crystal X-ray diffraction analysis. Numerical frequency calculations were performed to prove convergence at the local minimum after geometry optimization and to obtain the Gibbs free energy (293.15 K). The geometry of tetramethylsilane (TMS) was optimized as described above. Relaxed energy scans were performed in  $10^\circ$  steps by an increase in the C–N–N–C torsion angle in the range from 0 to  $180^\circ$ . The crystal structures of **2'**, **2''**, and  $\text{SiCl}_2(\text{oxinate})_2$  were optimized with TURBOMOLE rev. V7-7-1 [72] using the restricted PBE functional with a basis set pob-TZVP and RI-J auxiliary basis set for all atoms. A grid size of m4 and atom-pairwise dispersion correction with the Becke–Johnson damping scheme (D3BJ) [70,71] were used. During the periodic boundary optimization, the redundant coordinates and cell parameters were optimized. NMR chemical shifts were calculated with ADF-2019.303 [73] and referenced as described in the main text using a PBE function and an all-electron basis set TZ2P for all atoms [74] and spin-orbit relativistic ZORA Hamiltonian. Graphics were generated using Chemcraft [75].



### 3.2. Syntheses and Characterization

#### Compound 2' (C<sub>10</sub>H<sub>8</sub>Cl<sub>4</sub>N<sub>8</sub>Si).

Route A: Under a dry argon atmosphere, into a Schlenk flask with a magnetic stirring bar were added chloroform (15 mL), **1** (0.441 g, 3.67 mmol), and SiCl<sub>4</sub> (0.478 g, 2.81 mmol) at room temperature with stirring. The resultant mixture was stored at room temperature, and crystals of **2'** formed in the course of one day. Thereupon, the supernatant was removed by decantation, and the crystals were dried in a vacuum. Yield: 0.313 g (0.76 mmol, 42%) of **2'**. Elemental analysis calculated for C<sub>10</sub>H<sub>8</sub>Cl<sub>4</sub>N<sub>8</sub>Si (410.13 g·mol<sup>-1</sup>): C, 29.29%; H, 1.97%; N, 27.32%; found C, 29.34%; H, 1.84%; N, 26.55%. <sup>13</sup>C CP/MAS NMR: δ<sub>iso</sub> (ppm) 156.0 (C<sup>4</sup>), 150.0, 148.8 (C<sup>2,6</sup>), 116.1, 113.8 (C<sup>3,5</sup>); <sup>29</sup>Si CP/MAS NMR: δ<sub>iso</sub> (ppm) -177.4.

Route B: Under a dry argon atmosphere, a Schlenk flask was charged with toluene (5 mL) and **1** (0.294 g, 2.45 mmol). Via glass pipe, this flask was connected to a second Schlenk flask, which contained SiCl<sub>4</sub> (0.533 g, 3.14 mmol). This setup was stored at room temperature to allow for the diffusion of SiCl<sub>4</sub> into the toluene solution of **1** via the gas phase. In the course of some days, crystals of **2'** formed (confirmed by determination of the unit cell parameters by single-crystal X-ray diffraction).

Route C: Under a dry argon atmosphere, a Schlenk flask was charged with a magnetic stirring bar, toluene (15 mL), and SiCl<sub>4</sub> (0.537 g, 3.16 mmol), and the mixture was stirred at -78 °C (in a dry ice/isopropanol bath). To the stirred mixture, **1** (0.447 g, 3.72 mmol) was added dropwise, whereupon precipitation of a white solid commenced. Stirring at -78 °C was continued for 1 h, followed by stirring in an ice bath for 30 min, whereupon the cold dispersion was filtered. The solid product was washed with 3 × 1.5 mL of cold toluene (cooled in an ice bath) and dried in a vacuum. Yield: 0.70 g (1.71 mmol, 92%) of **2'**. <sup>13</sup>C CP/MAS NMR spectroscopy confirmed the formation of modification **2'** (cf. Figure S7 in the Supporting Information).

Compound **2''** (C<sub>10</sub>H<sub>8</sub>Cl<sub>4</sub>N<sub>8</sub>Si). Under a dry argon atmosphere, into a Schlenk flask with a magnetic stirring bar were added chloroform (15 mL), **1** (0.441 g, 3.67 mmol), and SiCl<sub>4</sub> (0.503 g, 2.96 mmol) at room temperature with stirring. The resultant mixture was stored in a freezer at -39 °C, and crystals of **2''** formed in the course of one day. Thereupon, the supernatant was removed by decantation, and the crystals were dried in a vacuum. Yield: 0.654 g (1.59 mmol, 87%) of **2''**. Elemental analysis calculated for C<sub>10</sub>H<sub>8</sub>Cl<sub>4</sub>N<sub>8</sub>Si (410.13 g·mol<sup>-1</sup>): C, 29.29%; H, 1.97%; N, 27.32%; found C, 29.00%; H, 1.83%; N, 26.28%. <sup>13</sup>C CP/MAS NMR: δ<sub>iso</sub> (ppm) 154.6 (C<sup>4</sup>), 151.2, 147.4 (C<sup>2,6</sup>), 115.0, 113.7 (C<sup>3,5</sup>); <sup>29</sup>Si CP/MAS NMR: δ<sub>iso</sub> (ppm) -177.8.

Compounds **1,4-3** and **1,5-3** (C<sub>13</sub>H<sub>10</sub>N<sub>4</sub>). For the series of experiments listed in Table 3: Under a dry argon atmosphere, into a Schlenk tube with a magnetic stirring bar were added 5 mL of the respective solvent (toluene or p-xylene), phenylacetylene (0.50 mL, ca. 4.6 mmol) and the respective amount of **1** (ca. 3.2–3.9 mmol). This solution was then placed in an oil bath at the temperature listed in Table 3 (110 °C for toluene solutions, 140 °C for p-xylene solutions) and stirred at this temperature for 0.5 or 2 h. Thereafter, the oil bath was removed, and the Schlenk tube was stored undisturbed for cooling to room temperature and for crystallization of the product. After 1 d, the crystalline product was separated from the supernatant by filtration, washing with the respective solvent (2 mL), and drying in a vacuum. The yields are given in Table 3, and the sets of <sup>1</sup>H and <sup>13</sup>C NMR spectra are similar to one another. As an example, see Figure 8. The positions of the signals are in accordance with those reported in the literature [54]. For a representative sample, an elemental analysis was performed, calculated for C<sub>13</sub>H<sub>10</sub>N<sub>4</sub> (222.25 g·mol<sup>-1</sup>): C, 70.26%; H, 4.54%; N, 25.21%; found C, 70.69%; H, 4.21%; N, 25.06%.

## 4. Conclusions

4-Azidopyridine forms adducts with SiCl<sub>4</sub> (SiCl<sub>4</sub>(4-azidopyridine)<sub>2</sub> **2**). Investigation of these compounds gave rise to the first crystallographically characterized example of an idealized D<sub>2d</sub> symmetric silane-pyridine adduct **2''** (i.e., the staggered configuration of the *trans*-disposed pyridine ligands at the hexacoordinate Si atom). Furthermore, the



$D_{2h}$  symmetric conformer **2'** (i.e., eclipsed configuration of the *trans*-disposed pyridine ligands at the hexacoordinate Si atom), which represents the “commonly encountered” configuration of this kind of silicon complexes, was also available as a crystalline solid. This pair **2'** and **2''** of conformers (and crystalline modifications) allowed for experimental comparison of such isomers of silane–pyridine-complexes for the first time. As shown by solid-state  $^{29}\text{Si}$  NMR spectroscopy, the relative conformations of the pyridine ligands exert particular influence on the features span  $\Omega$  and skew  $\kappa$  of the CSA tensor, whereas the isotropic chemical shift is practically identical. Thus, the observation of the same isotropic  $^{29}\text{Si}$  chemical shift for two solid samples of the presumably same compound does not guarantee that two samples of the same modification or of the same isomer have been obtained. Spinning side band spectra may reveal surprising differences and give rise to the discovery of new modifications or isomers. In this sense, the current study complements a similar result from a previous study of hexacoordinate Si complexes of the type  $\text{Ph}_2\text{Si}(\text{pyS})_2$  (pyS = pyridine-2-thiolate) [76]. Therein, two different isomers of  $\text{Ph}_2\text{Si}(\text{pyS})_2$  were encountered (with all-*cis*- $\text{C}_2\text{S}_2\text{N}_2$  and with *trans*- $\text{S}_2$ -*cis*- $\text{C}_2\text{N}_2$  Si coordination sphere), and these isomers as crystalline solids also exhibit very similar isotropic  $^{29}\text{Si}$  NMR shifts (−127.2 vs. −127.3 ppm) but different span (53.6 vs. 44.6 ppm) and different skew (+0.51 vs. −0.53) of the CSA tensor.

Computational analyses of the energetic differences between **2'** and **2''** revealed that **2''** should be as stable as **2'** as an isolated molecule (at least in a chloroform environment). In their respective crystal environment, however, **2'** is markedly more stable than **2''**, thus attributing the stability of the former to packing efficiency and the crystallization of the latter to the kinetics of crystallization.

Whereas in many previous studies (cf. examples and literature cited in the introduction), the coordination chemistry of silane–pyridine adducts has been studied, and the substituents at the pyridine ligands (such as alkyl, vinyl, aryl, Br, and  $\text{NMe}_2$ ) had merely played roles as spectator groups or substituents for electronic tuning of the pyridine *N*-donor properties, the azido substituent at the pyridine ligand offered an entry into studies of reactivities of such complexes and their free pyridine ligands. The example reaction of our study, i.e., (3+2)-cycloaddition of azido group and phenylacetylene, proved the beneficial influence of the presence of the  $\text{SiCl}_4$  moiety on this reaction. Both enhanced reaction rate and enhanced selectivity in favor of the formation of the 1-(4-pyridyl)-5-phenyl-1,2,3-triazole isomer (1,5-3) were observed. Thus, this study complements (3+2)-cycloadditions of Si-bound azido ligands and nitriles with the formation of Si-bound tetrazolyl groups [34].

Complexes of the type  $\text{SiX}_4(\text{azidopyridine})_2$  offer further intriguing potential for investigations to be carried out, yet. They include the investigation of oligomers or networks which feature silane–pyridine motifs. Azide-bridged Mn [77], Zn [78], and Cd complexes [79] were reported, which feature azide anions ( $\text{N}_3^-$ ) as bridging ligands in the network and 4-azidopyridine at the metal as terminal ligands (the  $\text{N}_3$ -moiety being a spectator group). Bridging thiocyanate ( $\text{SCN}^-$ ) and terminal 4-azidopyridine ligands were reported for Ni complexes [80]. Products of (3+2)-cycloadditions (some triazoles obtained from azidopyridines), however, may then serve as network-forming ligands as well, like in some Cd complexes [81], and bridges in macrocycles, like in some Ru complexes [82,83].

**Supplementary Materials:** The following supporting information can be downloaded at <https://www.mdpi.com/article/10.3390/inorganics11120473/s1>. Crystallographic data for the compounds reported in this paper (in CIF format) and a document containing the following: Raman spectra of **2'** and **2''** (Figures S1 and S2);  $^1\text{H}$ ,  $^{13}\text{C}$  and  $^{29}\text{Si}$  NMR spectra of **2'** in  $\text{CDCl}_3$  solution, with  $^1\text{H}$  and  $^{13}\text{C}$  spectra of **1** for comparison (Figures S3–S5),  $^{13}\text{C}$  solid state NMR spectra of **2'** and **2''** (Figures S6 and S7); molecular graphics and selected bond lengths and angles from the crystal structures of 1,4-3 and 1,5-3 (Figures S8 and S9, Tables S1 and S2); graphics of optimized molecular structures (isolated molecule and molecules in crystal packing) as well as the corresponding atomic coordinates for **2'** and **2''** (Figures S10–S13, Tables S3–S6); graphics of directions of  $^{29}\text{Si}$  CSA tensor principal axes for **2'** and **2''** (Figures S14 and S15); and a graphical representation of the development of these chemical shift principal values for **2'** and **2''** (Figure S16).

**Author Contributions:** Conceptualization, J.W.; investigation, S.R., M.G., D.G., E.B., R.G., and J.W.; writing—original draft preparation, J.W. and S.R.; writing—review and editing, S.R., E.B., R.G., E.K., and J.W.; visualization, S.R., R.G., and J.W.; supervision, E.K. and J.W. All authors have read and agreed to the published version of the manuscript.

**Funding:** This research was funded in part by the German Federal Ministry of Environment, Nature Conservation, Nuclear Safety and Consumer Protection (BMUV) under Project 1501667 (Am-BALL). Parts of this work were carried out with financial support from the European Union (European Social Fund, ESF) and the federal state of Saxony (Sächsische Aufbaubank, SAB, Dresden, Germany) via a Ph.D. scholarship (“Landesinnovationsstipendium”) to S. Riedel under Project 100380877-AP5.

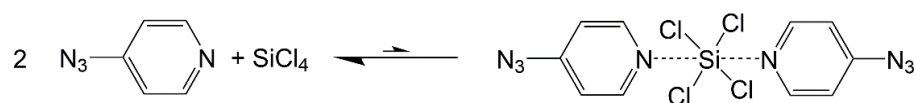
**Data Availability Statement:** CCDC 2302622 (2'), 2302624 (2''), 2302625 (1,4-3) and 2302623 (1,5-3) contain the supplementary crystal data for this article. These data can be obtained free of charge from the Cambridge Crystallographic Data Centre via <https://www.ccdc.cam.ac.uk/structures/> (accessed on 21 October 2023).

**Acknowledgments:** The authors are grateful to Marcel Swart (Institut de Química Computacional i Catalisi, Facultat de Ciències, Universitat de Girona, Spain) for his support with computational analyses (with the ADF package); to Michael Patzschke (Institute of Resource Ecology, Helmholtz-Zentrum Dresden-Rossendorf eV, D-01328 Dresden, Germany) for his support with computational analyses (with the Turbomole package); to Beate Kutzner (TU Bergakademie Freiberg, Institut für Anorganische Chemie); to Heidrun Hahn (TU Bergakademie Freiberg, Institut für Analytische Chemie) for NMR spectroscopy service; and to Regina Moßig (TU Bergakademie Freiberg, Institut für Anorganische Chemie) for Raman spectroscopy service.

**Conflicts of Interest:** The authors declare no conflict of interest.

## Appendix A

The  $^1\text{H}$ ,  $^{13}\text{C}\{^1\text{H}\}$  and  $^{29}\text{Si}\{^1\text{H}\}$  NMR spectroscopic confirmation of the presence of 4-azidopyridine and  $\text{SiCl}_4$  in the  $\text{CDCl}_3$  solution of **2** (especially the  $^{29}\text{Si}$  NMR signal at  $-19$  ppm, which is characteristic for the tetracoordinate Si atom of  $\text{SiCl}_4$ ), and the crystallization of compound **2** from this solution, imply the existence of a coordination–dissociation equilibrium in this solution, which is markedly on the side of the components 4-azidopyridine and  $\text{SiCl}_4$  (). We probed if this equilibrium could be shifted noticeably toward the side of **2** in solution by the addition of an additional drop of 4-azidopyridine to the NMR sample. In a rapid exchange equilibrium (on the NMR time scale), shifting of the equilibrium toward the species with hexacoordinate Si atom should result in an upfield shift of the average  $^{29}\text{Si}$  NMR signal. However, the  $^{29}\text{Si}$  NMR signal remains at essentially the same chemical shift. The addition of a greater excess of 4-azidopyridine was not helpful as it induced precipitation of compound **2** from the sample. The  $^{13}\text{C}\{^1\text{H}\}$  NMR spectra are more indicative of an effect of the presence of  $\text{SiCl}_4$  in the solution of 4-azidopyridine: Figure A1 shows the  $^{13}\text{C}\{^1\text{H}\}$  NMR spectra of 4-azidopyridine (**a**) and complex **2'** (**b**) in  $\text{CDCl}_3$  solution, and an upfield shift of the  $^{13}\text{C}$  signal of the pyridine 2,6-positions as well as a downfield shift of the signal of the pyridine 4-position is observed for the solution of **2'**. The relative directions of chemical shift change in these two signals are in accordance with the final positions of these signals for silicon complex **2** (as determined for **2'** and **2''** in the solid state, in which the signal of the pyridine 4-position is eventually more downfield shifted than the signals of the C atoms in 2,6-positions, cf. Figure 6).



**Scheme A1.** Dissociation and formation of **2** in solution.

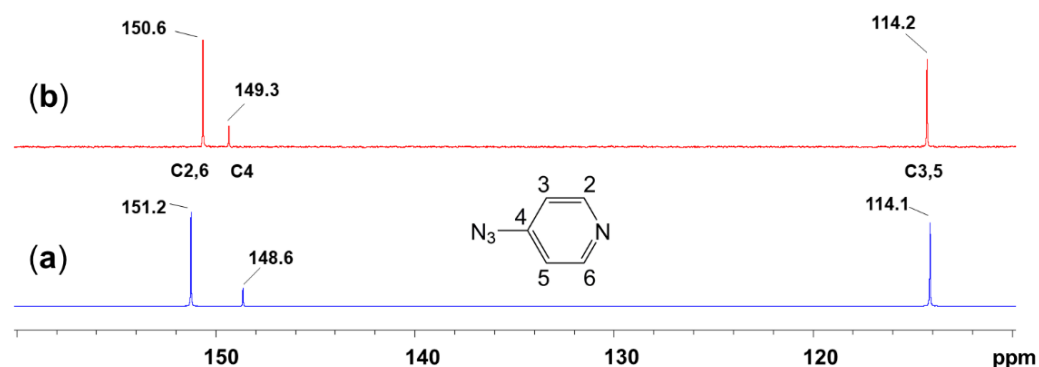


**Figure A1.**  $^{13}\text{C}\{^1\text{H}\}$  NMR spectra of  $\text{CDCl}_3$  solutions (referenced to internal TMS at 0 ppm) of (a) 4-azidopyridine and (b) complex  $2'$  with signal assignment. (In solution, the C atom positions 2,6 as well as 3,5 are chemically equivalent.).

## Appendix B

**Table A1.** Crystallographic data from data collection and refinement for  $2'$ ,  $2''$ , 1,4-3 and 1,5-3.

Parameter	$2'$	$2''$	1,4-3 <sup>1</sup>	1,5-3
Formula	$\text{C}_{10}\text{H}_8\text{Cl}_4\text{N}_8\text{Si}$	$\text{C}_{10}\text{H}_8\text{Cl}_4\text{N}_8\text{Si}$	$\text{C}_{13}\text{H}_{10}\text{N}_4$	$\text{C}_{13}\text{H}_{10}\text{N}_4$
$M_r$	410.13	410.13	222.25	222.25
$T$ (K)	200(2)	200(2)	180(2)	180(2)
$\lambda$ (Å)	0.71073	0.71073	0.71073	0.71073
Crystal system	monoclinic	monoclinic	triclinic	monoclinic
Space group	$P2_1/n$	$C2/c$	$P\bar{1}$	$P2_1/n$
$a$ (Å)	7.2920(6)	8.4988(8)	5.6770(4)	9.1259(3)
$b$ (Å)	10.7627(6)	17.5628(15)	7.1648(5)	11.9037(3)
$c$ (Å)	10.0442(8)	11.3833(11)	13.4102(11)	9.7351(4)
$\alpha$ (°)	90	90	75.071(6)	90
$\beta$ (°)	94.795(6)	101.860(7)	79.636(6)	99.034(3)
$\gamma$ (°)	90	90	89.686(6)	90
$V$ (Å <sup>3</sup> )	785.53(10)	1662.8(3)	517.96(7)	1044.42(6)
$Z$	2	4	2	4
$\rho_{\text{calc}}$ (g·cm <sup>-3</sup> )	1.73	1.64	1.43	1.41
$\mu_{\text{MoK}\alpha}$ (mm <sup>-1</sup> )	0.8	0.8	0.1	0.1
$F(000)$	412	824	232	464
$\theta_{\text{max}}$ (°), $R_{\text{int}}$	28.0, 0.0224	32.0, 0.0285	26.0, 0.0914 <sup>2</sup>	28.0, 0.0400
Completeness	100%	100%	100%	100%
Reflns collected	12304	14498	7244	21427
Reflns unique	1895	2896	2017	2508
Restraints	0	0	0	0
Parameters	107	106	156	155
GoF	1.277	1.082	1.052	1.075
$R1, wR2$ [ $I > 2\sigma(I)$ ]	0.0320, 0.0720	0.0290, 0.0669	0.0488, 0.1226	0.0374, 0.0897
$R1, wR2$ (all data)	0.0386, 0.0770	0.0413, 0.0723	0.0707, 0.1323	0.0421, 0.0922
Largest peak/hole (e·Å <sup>-3</sup> )	0.33, -0.29	0.43, -0.28	0.22, -0.22	0.27, -0.19

<sup>1</sup> The data set of compound 1,4-3 was collected from a twinned crystal (1 0 0, 0.137 -1 0, 0.853 0 -1), and the structure was refined as a two-domain twin using a HKLF5 format data set, which contained isolated reflections of the predominant domain and overlapping reflections. The batch scale factor (twin population) refined to 0.472(3).

<sup>2</sup> The ShelXL2018/03 refinement output of this HKLF5 twin refinement did not report  $R_{\text{int}}$  of the data set. The CheckCIF structure factor report lists  $R_{\text{int}} = 0.0914$ .

## Appendix C

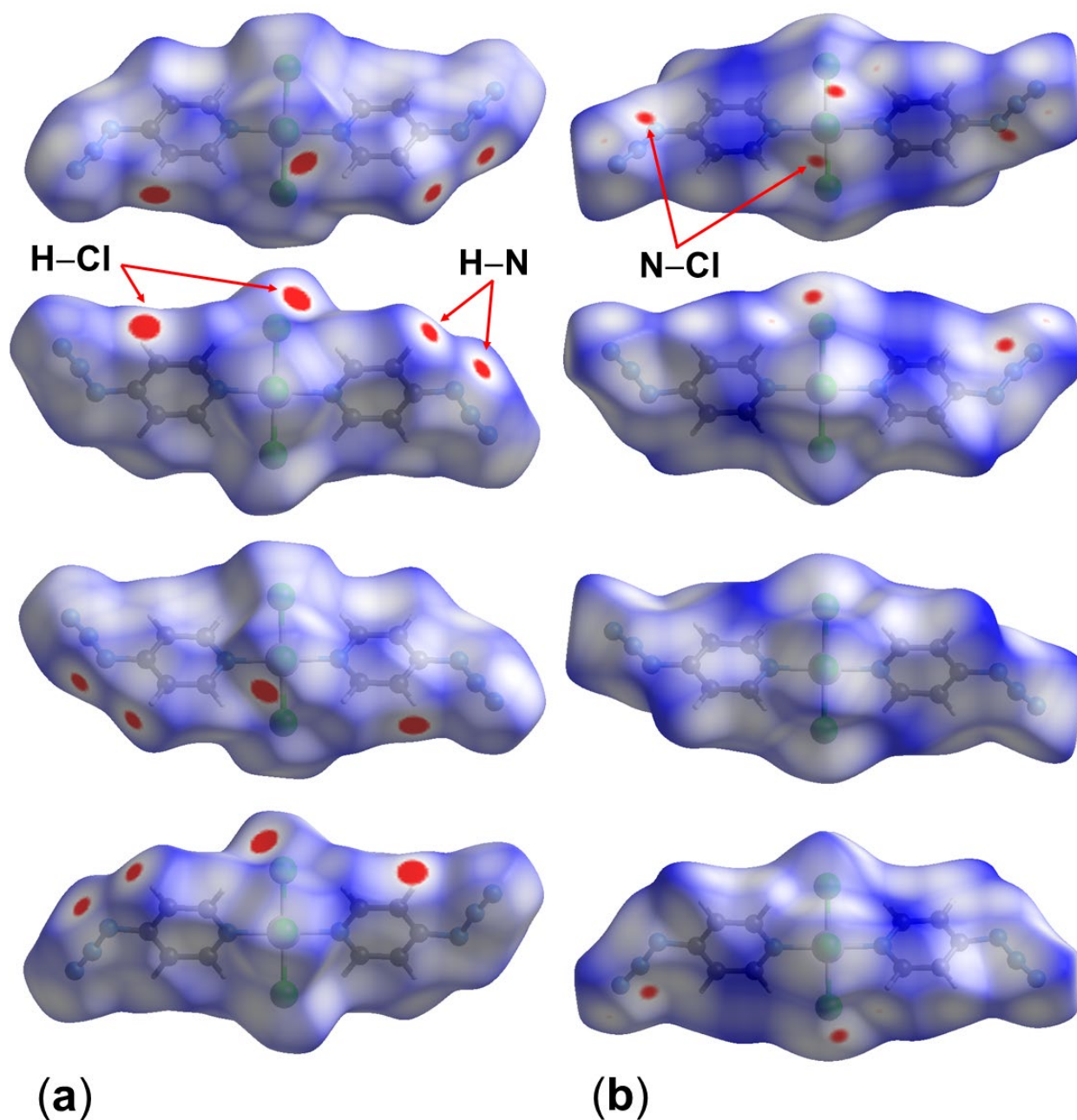


**Figure A2.** Isosurface plots (color scaled to  $d_{\text{norm}}$  range  $-0.05$  to  $+1.20$ ) of the Hirshfeld surface analyses (performed with CrystalExplorer version 21.5, revision 608bb32 [84]) of (a) the crystal structure of **2'** and (b) the crystal structure of **2''**. The four perspectives correspond to views along the four Cl-Si bonds of each molecule (i.e., from top to bottom, the four images represent steps of  $90^\circ$  rotation of the molecule about the horizontal N-Si-N axis). In **2'**, the predominant intermolecular contacts are established by  $\text{H}\cdots\text{N}$ - and  $\text{H}\cdots\text{Cl}$ -contacts, which are found on two opposite sides of the molecule. The full  $d_{\text{norm}}$  range is from  $-0.194$  to  $+1.054$ , the closest  $\text{H}\cdots\text{Cl}$ -contacts correspond to  $d_{\text{norm}} -0.194$ , the closest  $\text{H}\cdots\text{N}$ -contacts to  $d_{\text{norm}} -0.112$ . In the structure of **2''** the full  $d_{\text{norm}}$  range is from  $-0.061$  to  $+1.441$ ; the red areas (points of close contacts) represent  $\text{N}\cdots\text{Cl}$ -contacts at  $d_{\text{norm}} -0.061$ . They are found on one side of the molecule only.

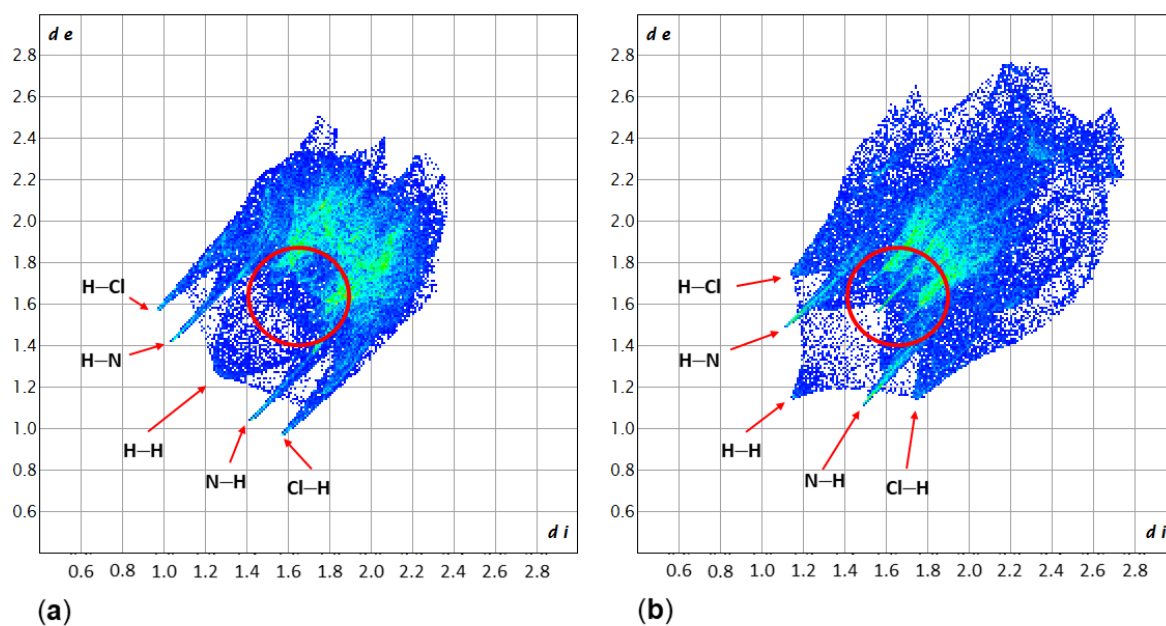


**Figure A3.** Fingerprint plots ( $d_e$  vs.  $d_i$ ) of the Hirshfeld surface analyses (performed with CrystalExplorer version 21.5, revision 608bb32 [84]) of (a) the crystal structure of **2'** and (b) the crystal structure of **2''**. In **2'**, the intermolecular contacts are established at shorter interatomic separations in general (the features of the map are shifted to shorter  $d_e$ ,  $d_i$  values), and pronounced interactions are found with  $H\cdots N$ - and  $H\cdots Cl$ -contacts. In the structure of **2''**, some shorter  $N\cdots N$ - and  $N\cdots Cl$ -contacts are characteristic of the packing (features inside the red circle in Figure 3b), which are not encountered with **2'** (cf. the red circle in Figure 3a).

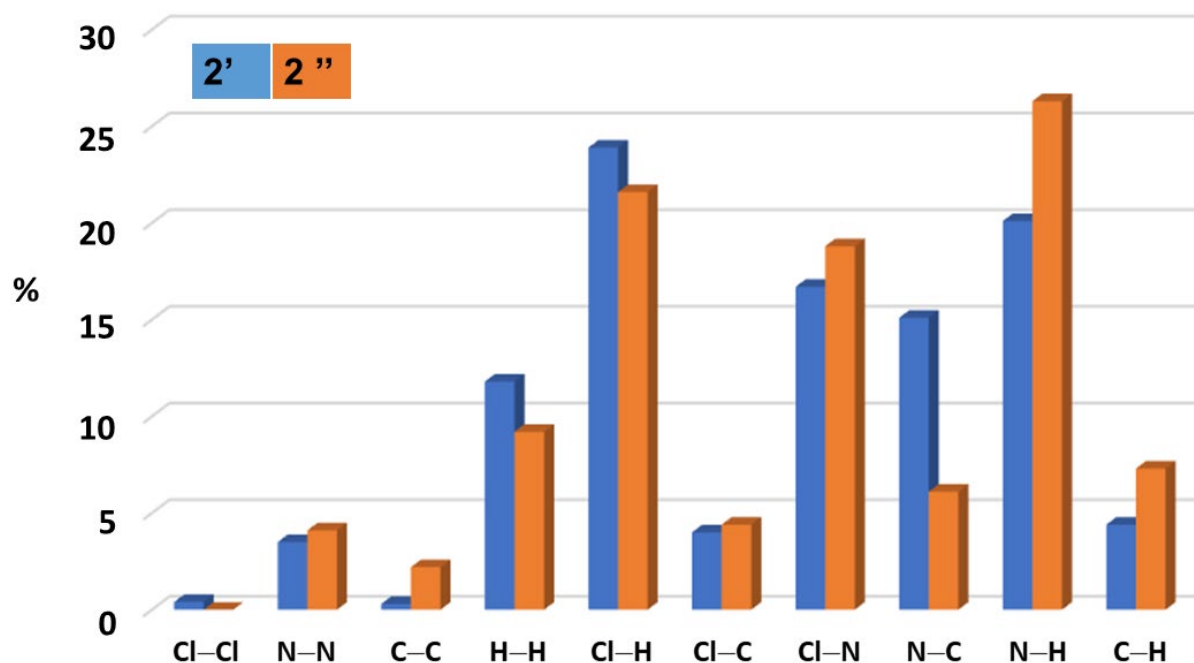


**Figure A4.** Percentage distribution (with respect to the area on the Hirshfeld surface) of the intermolecular contacts of **2'** and **2''**.



## Appendix D

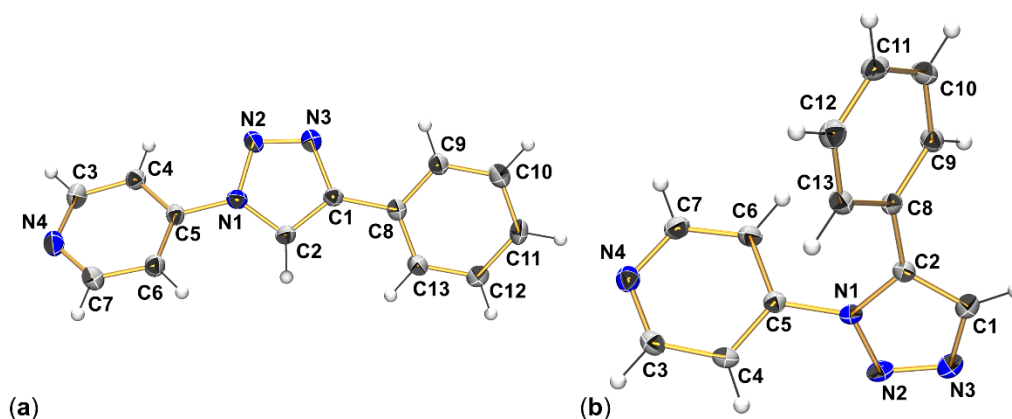


**Figure A5.** Molecular structures of (a) 1,4-3 and (b) 1,5-3 with thermal displacement ellipsoids at the 50% probability level and labels of non-hydrogen atoms.

## References

- Sivaramakrishna, A.; Pete, S.; Mhaskar, C.M.; Ramann, H.; Ramanaiah, D.V.; Arbaaz, M.; Niyaz, M.; Janardan, S.; Suman, P. Role of hypercoordinated silicon(IV) complexes in activation of carbon–silicon bonds: An overview on utility in synthetic chemistry. *Coord. Chem. Rev.* **2023**, *485*, 215140. [[CrossRef](#)]
- Singh, G.; Kaur, G.; Singh, J. Progressions in hyper-coordinate silicon complexes. *Inorg. Chem. Commun.* **2018**, *88*, 11–20. [[CrossRef](#)]
- Lemière, G.; Millanvois, A.; Ollivier, C.; Fensterbank, L. A Parisian Vision of the Chemistry of Hypercoordinated Silicon Derivatives. *Chem. Rec.* **2021**, *21*, 1119–1129. [[CrossRef](#)] [[PubMed](#)]
- Wagler, J.; Böhme, U.; Kroke, E. Higher-Coordinated Molecular Silicon Compounds. In *Functional Molecular Silicon Compounds I—Regular Oxidation States*; Scheschkewitz, D., Ed.; Springer: Berlin/Heidelberg, Germany, 2013; Volume 115, pp. 29–105. [[CrossRef](#)]
- Chuit, C.; Corriu, R.J.P.; Reye, C.; Young, J.C. Reactivity of Penta- and Hexacoordinate Silicon Compounds and Their Role as Reaction Intermediates. *Chem. Rev.* **1993**, *93*, 1371–1448. [[CrossRef](#)]
- Peloquin, D.M.; Schmedake, T.A. Recent advances in hexacoordinate silicon with pyridine-containing ligands: Chemistry and emerging applications. *Coord. Chem. Rev.* **2016**, *323*, 107–119. [[CrossRef](#)]
- Davy, J. XVIII. An Account of some Experiments on different Combinations of Fluoric Acid. *Philos. Trans. R. Soc. Lond.* **1812**, *102*, 352–369. [[CrossRef](#)]
- Plitzko, C.; Meyer, G. Synthesis and Crystal Structures of  $\text{NH}_4[\text{Si}(\text{NH}_3)\text{F}_5]$  and  $[\text{Si}(\text{NH}_3)_2\text{F}_4]$ . *Z. Anorg. Allg. Chem.* **1996**, *622*, 1646–1650. [[CrossRef](#)]
- Chen, F.; Hector, A.L.; Levason, W.; Reid, G.; Webster, M.; Zhang, W. Preparation and structure of the unique silicon(IV) cation  $[\text{SiF}_3(\text{Me}_3\text{tacn})]^+$ . *Chem. Commun.* **2009**, *45*, 1334–1336. [[CrossRef](#)]
- Tillmann, J.; Meyer-Wegner, F.; Nadj, A.; Becker-Baldus, J.; Sinke, T.; Bolte, M.; Holthausen, M.C.; Wagner, M.; Lerner, H.-W. Unexpected Disproportionation of Tetramethylethylenediamine-Supported Perchlorodisilane  $\text{Cl}_3\text{SiSiCl}_3$ . *Inorg. Chem.* **2012**, *51*, 8599–8606. [[CrossRef](#)]
- Bain, V.A.; Killeen, R.C.G.; Webster, M. The Crystal and Molecular Structure of Tetrafluorobis(pyridine)silicon(IV). *Acta Crystallogr. B* **1969**, *25*, 156–159. [[CrossRef](#)]
- Davydova, E.I.; Virovets, A.V.; Peresyphkina, E.V.; Timoshkin, A.Y. Crystal Structure of the Molecular Complex of Silicon Tetrafluoride with 4-Phenylpyridine. *Russ. J. Gen. Chem.* **2021**, *91*, 1964–1968. [[CrossRef](#)]
- Bechstein, O.; Ziemer, B.; Hass, D.; Trojanov, S.I.; Rybakov, V.B.; Maso, G.N. Halogen Exchange on Silicon Halides. XIII. Structure and Reactivity of Silicon Halide-Pyridine Compounds. *Z. Anorg. Allg. Chem.* **1990**, *582*, 211–216. [[CrossRef](#)]
- Hensen, K.; Mayr-Stein, R.; Spangenberg, B.; Bolte, M. Complexes of mixed silicon halides with 4-picoline. *Acta Crystallogr. C* **2000**, *56*, 610–613. [[CrossRef](#)]
- Bolte, M.; Hensen, K.; Spangenberg, B. Complexes of silicon tetrabromide with pyridine and 3,5-dimethylpyridine. *J. Chem. Crystallogr.* **2000**, *30*, 245–249. [[CrossRef](#)]
- Cheng, H.-J.; Lippe, K.; Kroke, E.; Wagler, J.; Fester, G.W.; Li, Y.-L.; Schwarz, M.R.; Saplinova, T.; Herkenhoff, S.; Ischenko, V.; et al. Sol-gel derived Si/C/O/N-materials: Molecular model compounds, xerogels and porous ceramics. *Appl. Organomet. Chem.* **2011**, *25*, 735–747. [[CrossRef](#)]
- Fester, G.W.; Wagler, J.; Brendler, E.; Böhme, U.; Roewer, G.; Kroke, E. Octahedral Adducts of Dichlorosilane with Substituted Pyridines: Synthesis, Reactivity and a Comparison of Their Structures and  $^{29}\text{Si}$  NMR Chemical Shifts. *Chem.-Eur. J.* **2008**, *14*, 3164–3176. [[CrossRef](#)]



18. Hensen, K.; Stumpf, T.; Bolte, M.; Näther, C.; Fleischer, H. Experimental Investigations and *ab Initio* Studies on Hexacoordinated Complexes of Dichlorosilane. *J. Am. Chem. Soc.* **1998**, *120*, 10402–10408. [[CrossRef](#)]
19. Fester, G.W.; Wagler, J.; Brendler, E.; Böhme, U.; Gerlach, D.; Kroke, E. Octahedral HSiCl<sub>3</sub> and HSiCl<sub>2</sub>Me Adducts with Pyridines. *J. Am. Chem. Soc.* **2009**, *131*, 6855–6864. [[CrossRef](#)]
20. Adley, A.D.; Bird, P.H.; Fraser, A.R.; Onyszczuk, M. The Crystal structures of 2,2'-Bipyridyltetrafluorosilicon(IV), 2,2'-Bipyridyltetrafluorogermanium(IV), and 2,2'-Bipyridyltetrafluorotin(VI). *Inorg. Chem.* **1972**, *11*, 1402–1409. [[CrossRef](#)]
21. Nakash, M.; Goldvaser, M.; Goldberg, I. Formation of Hexacoordinate Complexes of PhCCSiF<sub>3</sub> with 2,2'-Bipyridine and with 1,10-Phenanthroline through Intermolecular Silicon···Nitrogen Interactions. *Inorg. Chem.* **2004**, *43*, 5792–5794. [[CrossRef](#)]
22. Schwarze, N.; Kurscheid, B.; Steinhauer, S.; Neumann, B.; Stammeler, H.-G.; Ignat'ev, N.; Hoge, B. Synthesis of Functional Bis(pentafluoroethyl)silanes (C<sub>2</sub>F<sub>5</sub>)<sub>2</sub>SiX<sub>2</sub>, with X = H, F, Cl, Br, OPh, and O<sub>2</sub>CCF<sub>3</sub>. *Chem.-Eur. J.* **2016**, *22*, 17460–17467. [[CrossRef](#)]
23. Fester, G.W.; Eckstein, J.; Gerlach, D.; Wagler, J.; Brendler, E.; Kroke, E. Reactions of Hydridochlorosilanes with 2,2'-Bipyridine and 1,10-Phenanthroline: Complexation versus Dismutation and Metal-Catalyst-Free 1,4-Hydrosilylation. *Inorg. Chem.* **2010**, *49*, 2667–2673. [[CrossRef](#)]
24. Cruz-López, J.F.; Palacios-Chavez, J.A.; Guajardo-García, J.A.; González-García, A.; Báez, J.E.; López, J.A.; Orozco-Castellanos, L.M.; González-García, G. A straightforward synthesis of neutral hexacoordinated silicon(IV) complexes with SiN<sub>6</sub> skeleton. *Inorg. Chim. Acta* **2021**, *523*, 120406. [[CrossRef](#)]
25. Portius, P.; Davis, M. A new hexakis(isocyanato)silicate(IV) and the first neutral Lewis-base adducts of silicon tetrakisocyanate. *Dalton Trans.* **2010**, *39*, 527–532. [[CrossRef](#)]
26. Fleischer, H.; Hensen, K.; Stumpf, T. The First SiH<sub>2</sub><sup>2+</sup> Complex, Dihydridotetrakis(3-picoline)silicon Dichloride-Tetrakis(chloroform), [H<sub>2</sub>Si(3pic)<sub>4</sub>]Cl<sub>2</sub> · 4 CHCl<sub>3</sub>: Formation, Chemical Equilibria, and Structural Investigation by NMR Spectroscopy and Single-Crystal X-ray Diffraction. *Chem. Ber.* **1996**, *129*, 765–771. [[CrossRef](#)]
27. Hensen, K.; Mayr-Stein, R.; Rühl, S.; Bolte, M. *trans*-Dichlorotetrakis(4-methyl-pyridine)silicon bis(triiodide) chloroform solvate. *Acta Crystallogr. C* **2000**, *56*, 614–615. [[CrossRef](#)]
28. Hensen, K.; Mayr-Stein, R.; Rühl, S.; Bolte, M. *cis*-Bis(2,2'-bipyridyl-*N-N'*)dichlorosilicon diiodide. *Acta Crystallogr. C* **2000**, *56*, 607–609. [[CrossRef](#)]
29. Sawitzki, G.; von Schnering, H.G.; Kummer, D.; Seshadri, T. On the Structure of the Octahedral Cations *cis*-[SiX<sub>2</sub>(bipy)<sub>2</sub>]<sup>2+</sup>; the Crystal Structure of [Si(OH)<sub>2</sub>(bipy)<sub>2</sub>]I<sub>2</sub> · 2 H<sub>2</sub>O. *Chem. Ber.* **1978**, *111*, 3705–3710. [[CrossRef](#)]
30. Maguylo, C.; Chukwu, C.; Aun, M.; Monroe, T.B.; Ceccarelli, C.; Jones, D.S.; Merkert, J.W.; Donovan-Merkert, B.T.; Schmedake, T.A. Exploring the structure and redox activity of hexacoordinate bis(bipyridyl)silicon(IV) complexes. *Polyhedron* **2015**, *94*, 52–58. [[CrossRef](#)]
31. Hensen, K.; Kettner, M.; Bolte, M. Bromo(hydrido)methylbis(4-methylpyridine-*N*)silicon Bromide at 173K. *Acta Cryst. C* **1998**, *54*, 358–359. [[CrossRef](#)]
32. Hermannsdorfer, A.; Driess, M. Isolable Silicon-Based Polycations with Lewis Superacidity. *Angew. Chem. Int. Ed.* **2020**, *59*, 23132–23136. [[CrossRef](#)]
33. Portius, P.; Filippou, A.C.; Schnakenburg, G.; Davis, M.; Wehrstedt, K.-D. Neutral Lewis Base Adducts of Silicon Tetraazide. *Angew. Chem. Int. Ed.* **2010**, *49*, 8013–8016. [[CrossRef](#)]
34. Portius, P.; Davis, M. Synthesis of six-coordinate mono-, bis-, and tris(tetrazolato) complexes *via* [3 + 2] cycloadditions of nitriles to silicon-bound azido ligands. *Dalton Trans.* **2016**, *45*, 17141–17152. [[CrossRef](#)]
35. Kolb, H.C.; Finn, M.G.; Sharpless, K.B. Click Chemistry: Diverse Chemical Function from a Few Good Reactions. *Angew. Chem. Int. Ed.* **2001**, *40*, 2004–2021. [[CrossRef](#)]
36. L'abbé, G.; Beenaerts, L. Influence of electron-withdrawing N-1 substituents on the thermal behaviour of 5-azido-1,2,3-triazoles. *Tetrahedron* **1989**, *45*, 749–756. [[CrossRef](#)]
37. Colombano, G.; Travelli, C.; Galli, U.; Caldarelli, A.; Chini, M.G.; Canonico, P.L.; Sorba, G.; Bifulco, G.; Tron, G.C.; Genazzani, A.A. A Novel Potent Nicotinamide Phosphoribosyltransferase Inhibitor Synthesized via Click Chemistry. *J. Med. Chem.* **2010**, *53*, 616–623. [[CrossRef](#)]
38. Kwok, S.W.; Fotsing, J.R.; Fraser, R.J.; Rodionov, V.O.; Fokin, V.V. Transition-Metal-Free Catalytic Synthesis of 1,5-Diaryl-1,2,3-triazoles. *Org. Lett.* **2010**, *12*, 4217–4219. [[CrossRef](#)]
39. Timoshkin, A.Y.; Sevast'yanova, T.N.; Davydova, E.I.; Suvorov, A.V.; Schaefer, H.F. Quantum-Chemical Study of Adducts of Silicon Halides with Nitrogen-containing Donors: IV. Adducts with Pyridine. *Russ. J. Gen. Chem.* **2003**, *73*, 765–775. [[CrossRef](#)]
40. Wächtler, E.; Kämpfe, A.; Krupinski, K.; Gerlach, D.; Kroke, E.; Brendler, E.; Wagler, J. New Insights into Hexacoordinated Silicon Complexes with 8-Oxyquinolino Ligands: 1,3-Shift of Si-Bound Hydrocarbyl Substituents and the Influence of Si-Bound Halides on the 8-Oxyquinolino Coordination Features. *Z. Naturforsch. B* **2014**, *69*, 1402–1418. [[CrossRef](#)]
41. Herzfeld, J.; Berger, A.E. Sideband intensities in NMR spectra of samples spinning at the magic angle. *J. Chem. Phys.* **1980**, *73*, 6021–6030. [[CrossRef](#)]
42. Mason, J. Conventions for the reporting of nuclear magnetic shielding (or shift) tensors suggested by participants in the NATO ARW on NMR shielding constants at the University of Maryland, College Park, July 1992. *Solid State Nucl. Magn. Reson.* **1993**, *2*, 285–288. [[CrossRef](#)] [[PubMed](#)]
43. Soto, J.; Algarra, M.; Peláez, D. Nitrene formation is the first step of the thermal and photochemical decomposition reactions of organic azides. *Phys. Chem. Chem. Phys.* **2022**, *24*, 5109–5115. [[CrossRef](#)] [[PubMed](#)]

44. Wang, Y.-C.; Lai, X.-J.; Huang, K.; Yadav, S.; Qiu, G.; Zhang, L.; Zhou, H. Unravelling nitrene chemistry from acyclic precursors: Recent advances and challenges. *Org. Chem. Front.* **2021**, *8*, 1677–1693. [CrossRef]
45. Rao, H.S.P.; Chakibanda, G. Raney Ni catalyzed azide-alkyne cycloaddition reaction. *RSC Adv.* **2014**, *4*, 46040–46048. [CrossRef]
46. Jia, Z.; Zhu, Q. 'lick' assembly of selective inhibitors for MAO-A. *Bioorg. Med. Chem. Lett.* **2010**, *20*, 6222–6225. [CrossRef] [PubMed]
47. Kirmse, W.; Horner, L. Umsetzung von Phenylacetylen mit Aziden und Diazoverbindungen. *Justus Liebigs Ann. Chem.* **1958**, *614*, 1–3. [CrossRef]
48. El-Remaily, M.A.E.A.A.A.; Elhady, O.M. Iron (III)-porphyrin Complex FeTSP as an efficient catalyst for synthesis of tetrazole derivatives via [2 + 3] cycloaddition reaction in aqueous medium. *Appl. Organomet. Chem.* **2019**, *33*, e4989. [CrossRef]
49. Hermannsdorfer, A.; Driess, M. Silicon Tetrakis(trifluoromethanesulfonate): A Simple Neutral Silane Acting as a Soft and Hard Lewis Superacid. *Angew. Chem. Int. Ed.* **2021**, *60*, 13656–13660. [CrossRef]
50. Tschernuth, F.S.; Thorwart, T.; Greb, L.; Hanusch, F.; Inoue, S. Bis(perfluoropinacolato)silane: A Neutral Silane Lewis Superacid Activates Si–F Bonds. *Angew. Chem. Int. Ed.* **2021**, *60*, 25799–25803. [CrossRef]
51. Singh, M.S.; Chowdhury, S.; Koley, S. Advances of azide-alkyne cycloaddition-click chemistry over the recent decade. *Tetrahedron* **2016**, *72*, 5257–5283. [CrossRef]
52. Mazur, L.; Koziol, A.E.; Modzelewska-Banachiewicz, B. C-H...N contacts in 4-phenyl-3-(4-pyridyl)-4H-1,2,4-triazole. *Acta Crystallogr. E* **2004**, *60*, o2287–o2289. [CrossRef]
53. Jędrzejowski, D.; Pander, M.; Nitek, W.; Bury, W.; Matoga, D. Turning Flexibility into Rigidity: Stepwise Locking of Interpenetrating Networks in a MOF Crystal through Click Reaction. *Chem. Mater.* **2021**, *33*, 7509–7517. [CrossRef]
54. Chattopadhyay, B.; Vera, C.I.R.; Chuprakov, S.; Gevorgyan, V. Fused Tetrazoles as Azide Surrogates in Click Reaction: Efficient Synthesis of N-Heterocycle-Substituted 1,2,3-Triazoles. *Org. Lett.* **2010**, *12*, 2166–2169. [CrossRef]
55. Massiot, D.; Fayon, F.; Capron, M.; King, I.; Le Calvlé, S.; Alonso, B.; Durand, J.-O.; Bujoli, B.; Gan, Z.; Hoatson, G. Modeling one and two-dimensional Solid State NMR spectra. *Magn. Reson. Chem.* **2002**, *40*, 70–76. [CrossRef]
56. Sheldrick, G.M. SHELXT—Integrated space-group and crystal-structure determination. *Acta Crystallogr. A* **2015**, *71*, 3–8. [CrossRef]
57. Sheldrick, G.M. *Program for the Refinement of Crystal Structures*; SHELXL-2018/3; University of Göttingen: Göttingen, Germany, 2018.
58. Sheldrick, G.M. *Program for the Refinement of Crystal Structures*; SHELXL-2019/3; University of Göttingen: Göttingen, Germany, 2019.
59. Sheldrick, G. A short history of SHELX. *Acta Crystallogr. A* **2007**, *64*, 112–122. [CrossRef]
60. Sheldrick, G. Crystal structure refinement with SHELXL. *Acta Crystallogr. C* **2015**, *71*, 3–8. [CrossRef]
61. Farrugia, L.J. ORTEP-3 for windows—A version of ORTEP-III with a graphical user interface (GUI). *J. Appl. Crystallogr.* **1997**, *30*, 565. [CrossRef]
62. Farrugia, L.J. WinGX and ORTEP for Windows: An update. *J. Appl. Crystallogr.* **2012**, *45*, 849–854. [CrossRef]
63. POV-RAY (Version 3.7), Trademark of Persistence of Vision Raytracer Pty. Ltd., Williamstown, Victoria (Australia). Copyright Hallam Oaks Pty. Ltd., 1994–2004. Available online: <http://www.povray.org/download/> (accessed on 28 June 2021).
64. Macrae, C.F.; Sovago, I.; Cottrell, S.J.; Galek, P.T.A.; McCabe, P.; Pidcock, E.; Platings, M.; Shields, G.P.; Stevens, J.S.; Towler, M.; et al. Mercury 4.0: From visualization to analysis, design and prediction. *J. Appl. Cryst.* **2020**, *53*, 226–235. [CrossRef]
65. Neese, F. Software update: The ORCA program system—Version 5.0. *WIREs Comput. Mol. Sci.* **2022**, *8*, e1606. [CrossRef]
66. Weigend, F.; Ahlrichs, R. Balanced basis sets of split valence, triple zeta valence and quadruple zeta valence quality for H to Rn: Design and assessment of accuracy. *Phys. Chem. Chem. Phys.* **2005**, *7*, 3297–3305. [CrossRef] [PubMed]
67. Pantazis, D.A.; Neese, F. All-electron basis sets for heavy elements. *WIREs Comput. Mol. Sci.* **2014**, *4*, 363–374. [CrossRef]
68. van Lenthe, E.; Baerends, E.J.; Snijders, J.G. Relativistic regular two-component Hamiltonians. *J. Chem. Phys.* **1993**, *99*, 4597–4610. [CrossRef]
69. van Wüllen, C. Molecular density functional calculations in the regular relativistic approximation: Method, application to coinage metal diatomics, hydrides, fluorides and chlorides, and comparison with first-order relativistic calculations. *J. Chem. Phys.* **1998**, *109*, 392–399. [CrossRef]
70. Grimme, S.; Ehrlich, S.; Goerigk, L. Effect of the damping function in dispersion corrected density functional theory. *J. Comput. Chem.* **2011**, *32*, 1456. [CrossRef]
71. Grimme, S.; Antony, J.; Ehrlich, S.; Krieg, H. A consistent and accurate ab initio parametrization of density functional dispersion correction (DFT-D) for the 94 elements H–Pu. *J. Chem. Phys.* **2010**, *132*, 154104–154119. [CrossRef]
72. Balasubramani, S.G.; Chen, G.P.; Coriani, S.; Diedenhofen, M.; Frank, M.S.; Franzke, Y.J.; Furche, F.; Grotjahn, R.; Harding, M.E.; Hättig, C.; et al. TURBOMOLE: Modular program suite for ab initio quantum-chemical and condensed-matter simulations. *J. Chem. Phys.* **2020**, *152*, 184107. [CrossRef]
73. Te Velde, G.; Bickelhaupt, F.M.; Baerends, E.J.; Fonseca Guerra, C.; van Gisbergen, S.J.A.; Snijders, J.G.; Ziegler, T. Chemistry with ADF. *J. Comput. Chem.* **2001**, *22*, 931–967. [CrossRef]
74. van Lenthe, E.; Baerends, E.J. Optimized Slater-type basis sets for the elements 1–118. *J. Comput. Chem.* **2003**, *24*, 1142–1156. [CrossRef]
75. Chemcraft, Version 1.8 (Build 164). 2016. Available online: <http://www.chemcraftprog.com/> (accessed on 19 September 2015).

76. Seidel, A.; Weigel, M.; Ehrlich, L.; Gericke, R.; Brendler, E.; Wagler, J. Molecular Structures of the Silicon Pyridine-2-(thi)olates  $\text{Me}_3\text{Si}(\text{pyX})$ ,  $\text{Me}_2\text{Si}(\text{pyX})_2$  and  $\text{Ph}_2\text{Si}(\text{pyX})_2$  (py = 2-Pyridyl, X = O, S), and Their Intra- and Intermolecular Ligand Exchange in Solution. *Crystals* **2022**, *12*, 1054. [[CrossRef](#)]
77. Escuer, A.; Mautner, F.A.; Goher, M.A.S.; Abu-Youssef, M.A.M.; Vicente, R. A two-dimensional azido-based topologic ferrimagnet. *Chem. Commun.* **2005**, *41*, 605–607. [[CrossRef](#)]
78. Mautner, F.A.; Scherzer, M.; Berger, C.; Fischer, R.C.; Massoud, S.S. Synthesis, characterization and luminescence properties of zinc(II) complexes of pseudohalides and nitrite derived from 4-azidopyridine. *Inorg. Chim. Acta* **2015**, *425*, 46–51. [[CrossRef](#)]
79. Mautner, F.A.; Scherzer, M.; Berger, C.; Fischer, R.C.; Vicente, R.; Massoud, S.S. Synthesis and characterization of three new 1-D polymeric  $[\text{M}_2(4\text{-azidopyridine})_4(\mu_1,1\text{-N}_3)_2(\mu_1,3\text{-N}_3)_2]_n$  (M = Ni, Co, Cd) complexes. *Polyhedron* **2015**, *85*, 329–336. [[CrossRef](#)]
80. Mautner, F.A.; Scherzer, M.; Berger, C.; Fischer, R.C.; Vicente, R.; Massoud, S.S. Synthesis and characterization of five new thiocyanato- and cyanato-metal(II) complexes with 4-azidopyridine as co-ligand. *Polyhedron* **2015**, *85*, 20–26. [[CrossRef](#)]
81. Cisterna, J.; Araneda, C.; Narea, P.; Cárdenas, A.; Llanos, J.; Brito, I. The Positional Isomeric Effect on the Structural Diversity of Cd(II) Coordination Polymers, Using Flexible Positional Isomeric Ligands Containing Pyridyl, Triazole, and Carboxylate Fragments. *Molecules* **2018**, *23*, 2634. [[CrossRef](#)]
82. Singh, J.; Kim, D.H.; Kim, E.-H.; Singh, N.; Kim, H.; Hadiputra, R.; Jung, J.; Chi, K.-W. Selective and quantitative synthesis of a linear [3]catenane by two component coordination-driven self-assembly. *Chem. Commun.* **2019**, *55*, 6866–6869. [[CrossRef](#)]
83. Singh, J.; Park, D.W.; Kim, D.H.; Singh, N.; Kang, S.C.; Chi, K.-W. Coordination-Driven Self-Assembly of Triazole-Based Apoptosis-Inducible Metallomacrocycles. *ACS Omega* **2019**, *4*, 10810–10817. [[CrossRef](#)]
84. Spackman, P.R.; Turner, M.J.; McKinnon, J.J.; Wolff, S.K.; Grimwood, D.J.; Jayatilaka, D.; Spackman, M.A. CrystalExplorer: A program for Hirshfeld surface analysis, visualization and quantitative analysis of molecular crystals. *J. Appl. Cryst.* **2021**, *54*, 1006–1011. [[CrossRef](#)]

**Disclaimer/Publisher's Note:** The statements, opinions and data contained in all publications are solely those of the individual author(s) and contributor(s) and not of MDPI and/or the editor(s). MDPI and/or the editor(s) disclaim responsibility for any injury to people or property resulting from any ideas, methods, instructions or products referred to in the content.